



Minerva Access is the Institutional Repository of The University of Melbourne

Author/s:

Ren, J;Zhang, L;Walkley, B;Black, JR;San Nicolas, R

Title:

Degradation resistance of different cementitious materials to phosphoric acid attack at early stage

Date:

2022-01-01

Citation:

Ren, J., Zhang, L., Walkley, B., Black, J. R. & San Nicolas, R. (2022). Degradation resistance of different cementitious materials to phosphoric acid attack at early stage. *Cement and Concrete Research*, 151, <https://doi.org/10.1016/j.cemconres.2021.106606>.

Persistent Link:

<https://hdl.handle.net/11343/292043>

Degradation resistance of different cementitious materials to phosphoric acid attack at early stage

Jie Ren^{1,2}, Lihai Zhang¹, Brant Walkley³, Jay R. Black⁴, Rackel San Nicolas^{1*}

¹ Department of Infrastructure Engineering, the University of Melbourne, Victoria, 3010, Australia

² Guangdong Provincial Key Laboratory of Durability for Marine Civil Engineering, College of Civil and Transportation Engineering, Shenzhen University, Shenzhen 518060, China

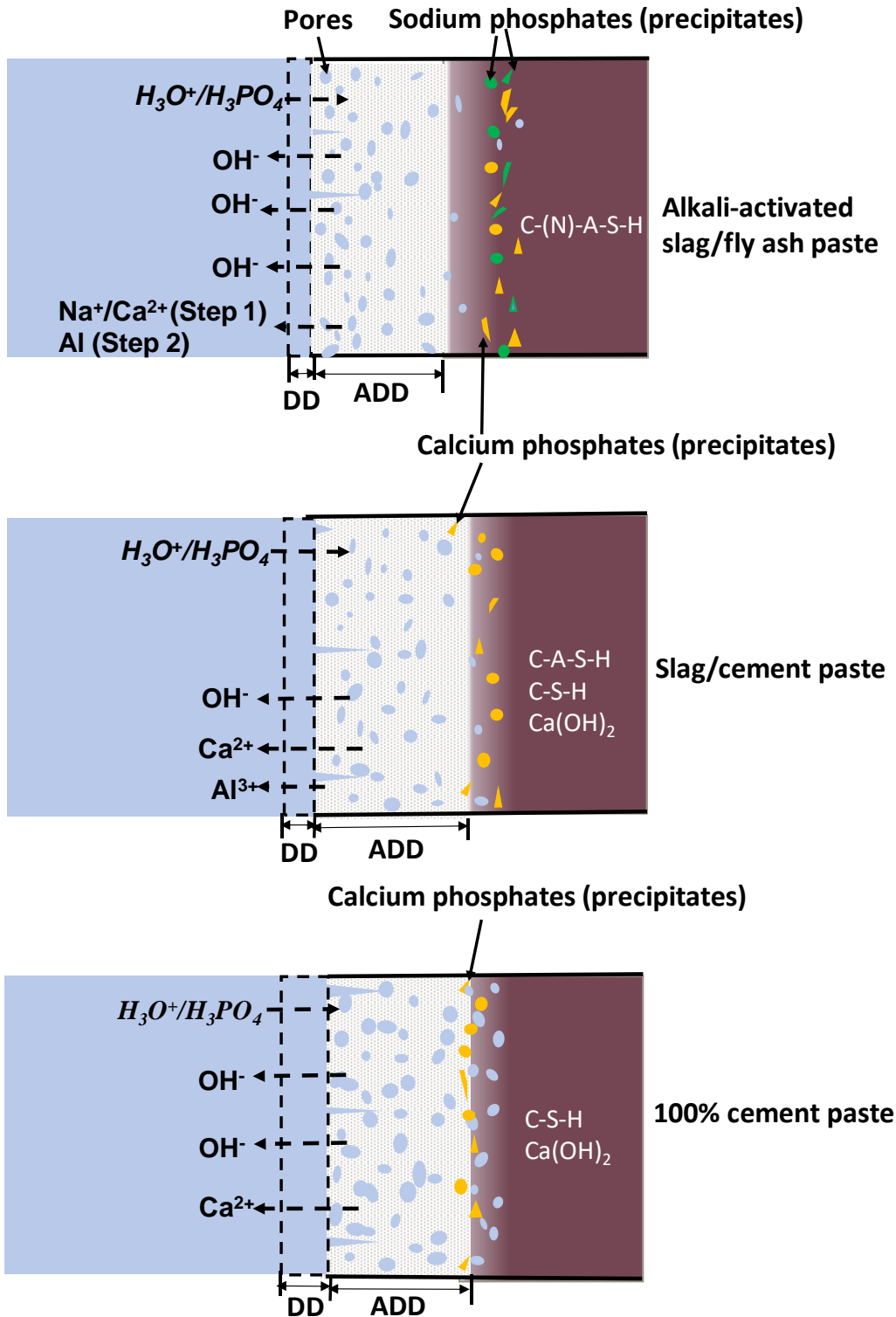
³ Department of Chemical and Biological Engineering, The University of Sheffield, Sheffield S1 3JD, UK

⁴ School of Earth Sciences, Peter Cook Centre for CCS Research, The University of Melbourne, VIC 3010 Australia

Abstract

Sewer wastewater systems pose great threats to OPC-based concretes used for pipes due to the presence of various acids. Phosphoric acid can cause as much damage as sulphuric acid but has been very lightly studied. This study focuses on the early stage of the degradation process of different cementitious materials in phosphoric acid. Three types of cementitious materials are compared: OPC (100% cement), slag-blended OPC (slag/cement mass ratio at 65/35) and alkali-activated slag/fly ash pastes (slag/fly ash mass ratio at 50/50). Samples were exposed to phosphoric acid solution with a constant pH at 2.0 ± 0.2 for 44 days. The degradation kinetics, chemical and microstructural properties as well as dissolution rate of these binders are analysed. The results show that the alkali-activated slag/fly ash binder has the lowest degradation rate compared to the other cement-based binders. The intrinsic characteristics of the binders lead to significant changes in the kinetics of degradation. The chemical properties of the binders are the critical influential factor of the early stage behaviour. A conceptual degradation process is proposed to describe the early-stage kinetics of degradation for the cementitious materials studied.

Keywords: Phosphoric acid; Early stage; Alkali-activated slag/fly ash binders; Degradation resistance



28

29 **Graphical abstract**

30 Schematic diagram showing the early stage degradation processes of AASF and OPC-based
 31 pastes exposed to the phosphoric acid. ADD-Apparent degradation depth; DD-
 32 Dissolved/detached depth.

33 **1. Introduction**

34 The resistance of cementitious materials exposed to acidic environments, such as sewage
35 wastewater pipes containing effluents, has seen a recent growth in academic and industrial
36 interest [1-14] due to immense costs of maintaining this infrastructure. When exposed to acidic
37 agro-industrial wastewaters, cementitious materials suffer from severe deterioration due to
38 reactions between their alkaline matrix and various acids [15-19].

39 Phosphates (H_2PO_4^- , HPO_4^{2-} or PO_4^{3-}), are one of the main components in silage effluent
40 discharged by agricultural practices with a resultant acidic condition ($\text{pH} \approx 3.5-5$) [20], posing
41 severe challenges for cementitious materials used in sewer networks [8, 21, 22]. According to
42 related research [23], fertilizer production could produce a dilute mixture of phosphoric,
43 sulfuric and even fluosilic acids with pH level as low as 1 to 2. Previous studies have shown
44 that the exposure of OPC concretes to phosphoric acid ($\text{pH} = 2, 3$ or 4) or phosphate-rich acidic
45 environments resulted in significant degradation [1, 8, 24].

46 It has been reported that the degradation process of cementitious binders caused by acid
47 attacks is a synergistic effect of chemical reactions which generally dominate early stage
48 degradation and physical ion diffusion which is more obvious during later stages [25, 26].
49 Specially, chemical reactions occur at the surface of cementitious binders first, forming
50 different chemical products and a degraded layer. With the thickness of the degraded layer
51 gradually increasing, the acid solution has to diffuse the degraded layer before reaching
52 undegraded components and triggering new reactions. It is apparent the early stage degradation
53 process is critical for the entire performance of cementitious binders as it determines the
54 reaction products, i.e. different types of calcium salts, and formation of degraded layer which
55 could significantly influence the subsequent degradation evolutions [16, 27, 28]. Despite recent
56 advances, there remains a lack of understanding of the degradation effect and related
57 mechanisms of phosphoric acid on cementitious materials, particularly during early stages.

58 Alkali-activated materials (AAMs) are a viable alternative with potential to replace OPC-
59 based binders due to their lower CO_2 footprint, comparable mechanical strength and enhanced
60 durability, especially acid resistance compared to their OPC counterparts. Among all types of
61 AAMs, alkali-activated slag/fly ash (AASF) has become more appealing due to some
62 disadvantages and limitations when only fly ash (FA) or slag is used [29-32]. Specifically, the
63 use of FA as the only precursor often requires heat curing to achieve structural integrity at early
64 ages [33], which is not practical for in-situ industrial applications. For alkali-activated slag, the
65 main reaction product after hydration reaction is an aluminium-substituted calcium silicate

66 hydrate gel (C-(A)-S-H gel) with a low Ca/Si ratio [34]. This type of gel is reported to be more
67 susceptible towards acidic degradation due to its higher calcium content as compared to the
68 sodium aluminosilicate hydrate (N-A-S-H) type gels in FA-based AAMs [35, 36]. In
69 comparison, AASF binders contain both C-(A)-S-H and N-A-S-H gels [37-39] which are
70 expected to mitigate the abovementioned problems that single slag or FA-based AAMs have.

71 Durability of AASF binders in acid environments has been partially investigated in some
72 literature and it is confirmed that although AASF binders generally have a certain resistance
73 capacity towards some acid attacks such as sulphuric and nitric, they may still suffer from
74 severe deteriorations such as the formation of a degraded product layer along with corroded
75 depth. "Corroded depth" is here defined as in some literature as an area with lower pH and
76 other possible change in the nature of the binder [40-42]. However, related research focusing
77 on their behaviour under phosphoric acid attack and detailed comparisons with OPC-based
78 binders is far from adequate [8].

79 This study aims to investigate the early stage degradation of AASF (slag/FA = 1 by mass)
80 in phosphoric acid solutions and another two types of OPC-based binders are used as references.
81 The blended OPC binder usage is based on studies [19, 43] which reported that supplementary
82 cementitious materials rich in Al (such as slag in this study) could improve the acid resistance
83 by improving the microstructure and integrity of degraded layers. Various indicators including
84 degradation depth, mass changes and leaching rates of ions were employed in the study to
85 monitor the degradation kinetics. Chemical and microstructural analysis were also used to
86 characterise their resistance to degradation by phosphoric acid at early stages. Finally,
87 conceptual descriptions of the degradation for all binders are proposed.

88 **2. Materials and methods**

89 **2.1. Materials**

90 A type of FA (class F) according to ASTM C618 and grand granulated blast furnace slag
91 (GGBFS) were used as precursors for AASF binders, supplied by CEMENT AUSTRALIA and
92 Independent Cement and Lime Pty. Ltd., respectively. The FA and GGBFS has a specific
93 gravity of 2,800 and 2,200 kg/m³ respectively and their corresponding median particle size (d₅₀)
94 was 14 for FA and 25 µm for GGBFS. A GP (General purpose) type OPC (Eureka Cement,
95 Australia) in accordance with AS 3972 with a specific gravity between 2,800-3,200 kg/m³ and
96 bulk density 1,200-1,600 kg/m³ was used. Their chemical compositions and X-ray diffraction
97 (XRD) patterns are shown in Table 1 and Fig. 1 (FA and GGBFS) and Fig. 2 (OPC), respectively.
98 According to Fig. 1, FA contains some crystalline phases such as mullite, quartz and hematite.

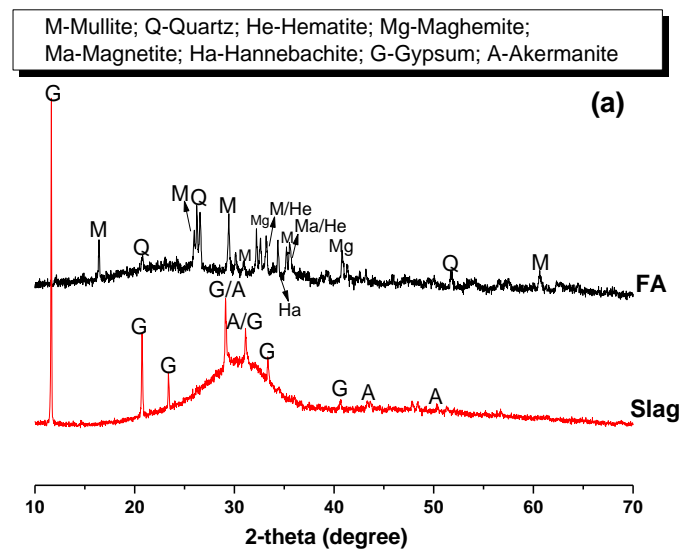
99 In comparison, GGBFS was mainly amorphous evidenced by a broad diffuse hump between
 100 25 and 35 ° (2θ) with a few Akermanite and gypsum. Generally, OPC is composed of alite,
 101 belite and gypsum as well as ferrite which are also observed in Fig. 2. Anhydrous sodium
 102 metasilicate powder (Na₂SiO₃) with SiO₂:Na₂O molar ratio at 1:1 was selected as the solid
 103 alkaline activator which was provided by Redox Pty Ltd. Tap water was used as the mixing
 104 water. Phosphoric acid solution was synthesised by mixing distilled water and analytical
 105 reagent-grade ortho-phosphoric acid (85% w/w, 1.71 g/mL), provided by Chem-supply.

106 **Table 1**

107 Chemical compositions of the FA, GGBFS and OPC used (wt.%), as determined by X-ray
 108 fluorescence.

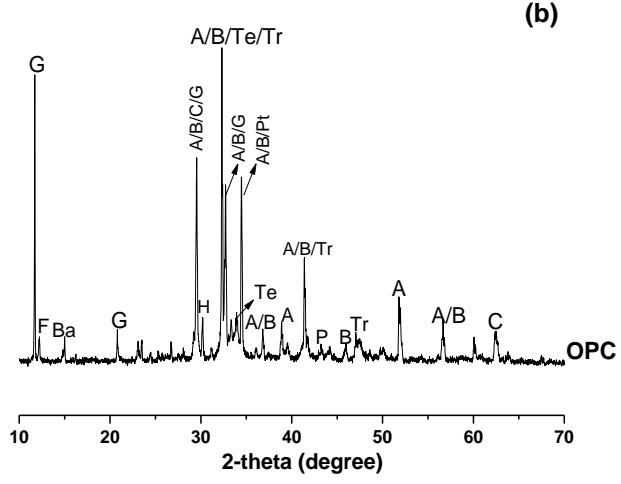
Precursor	Component (mass % as oxide)										
	SiO ₂	TiO ₂	Al ₂ O ₃	Fe ₂ O ₃	MnO	MgO	CaO	K ₂ O	P ₂ O ₅	SO ₃	LOI*
GGBFS	31.00	0.49	13.96	0.32	0.33	6.33	40.92	0.31	0.01	2.17	2.11
FA	42.09	1.44	25.13	13.16	0.18	1.27	13.56	0.41	1.10	0.41	0.81
OPC	20.34	-	4.47	4.58	-	1.24	62.91	0.29	-	2.58	3.27

109 * LOI refers to loss on ignition at 1,000 °C.



110

A-Alite(C_3S); B-Belite(C_2S); C-Calcite; Te- C_4AF ; Tr- C_3A ; H-Hemihydrate;
 G-Gypsum; P-Periclase; F-Ferrite; Ba-Bassanite; Pt-Portlandite



111

112

Fig. 1. XRD spectra of the raw materials: (a) Slag and FA; (b) OPC.

113

2.2. Preparation of AASF and OPC-based pastes

114

The AASF paste was prepared by mixing the GGBFS and FA dry powders first in a Hobart mixer for two minutes before adding the alkaline activator solution which was made by stirring the Na_2SiO_3 and required water in a beaker, then covered with a watch glass to minimise evaporation and followed by cooling down naturally to room temperature. The mixture was mixed for 8 minutes, cast in two layers into 50 mm cubic moulds or cylinder moulds (Φ 27.5 mm \times H 55 mm) and compacted carefully on a vibrating table for two minutes to remove introduced air bubbles during the mixing process. The newly-mixed pastes were cured at 23 ± 2 °C with plastic films covered on casting surfaces to minimise moisture loss. After 24 hours, all specimens were demoulded, sealed tightly in plastic bags and stored immediately in a cabinet at room temperature (23 ± 2 °C) until further testing. For OPC-based pastes, a pilot study was carried out in order to achieve similar compressive strength compared to that of the AASF paste. Pure 100% OPC paste and blended OPC with GGBFS were manufactured with the predetermined water-to-binder ratio at 0.38 and 0.40 respectively. The mixing procedure was similar compared to AASF pastes but the curing condition was different: OPC-based pastes were all cured in water with the same laboratory condition (temperature = 23 ± 2 °C). Detailed denotations and mix proportions of the three mixes are tabulated in Table 2. Paste samples were used throughout the study and were cured for 56 days to ensure a complete hydration process prior to acid immersions and other tests. It is noteworthy that pastes not mortar or concrete specimens were made for comparison because we mainly deal with the intrinsic

132

133 stabilities of different binding components in various binders when suffering from acid attacks
134 without considering interfacial transition zone.

135 **Table 2**

136 Mix proportions of the three types of binder mixes in the study.

Sample code	Composition (%) of the binder	Water/binder ratio	Solid activator dosage (%)
50Slag_50FA	GGBFS: FA = 50:50	0.342	8
65Slag_35OPC	GGBFS: OPC = 65:35	0.40	-
100OPC	OPC: 100	0.38	-

137 All ratios and percentages are expressed in mass.

138 **2.3. Test procedure**

139 **2.3.1. Initial properties before acid immersion**

140 Water absorption accompanied with volume of permeable voids (VPV) and capillary
141 sorptivity of the paste specimens after 56 days of curing[44] were measured according to
142 ASTM C642-06 [45] and ASTM C1585-04 [46], respectively. The preconditioning
143 temperature for the water absorption and VPV, and capillary sorptivity test was 60 °C and 50 °C
144 respectively because higher temperatures may alter the microstructures of alkali-activated
145 binders [44]. Final results were expressed as an average of three specimens for each mix. The
146 compressive strength after 56-day curing was tested on the 50 mm cubic samples in triplicates
147 using an ELE International tester with a loading rate at 0.9 kN/s in compliance with the ASTM
148 C109/C109M-12 (2012) [47].

149

150 **2.3.2. Phosphoric acid immersion**

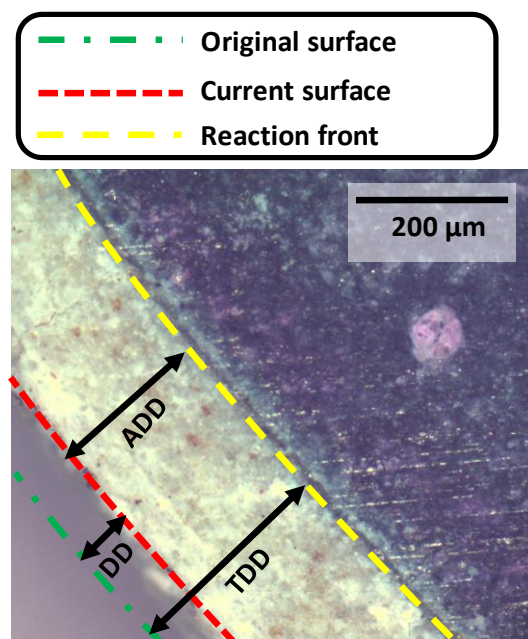
151 In this study, for each binder mix, six cylindrical samples were fully immersed in separated
152 containers with 1 L phosphoric acid ($\text{pH} = 2.0 \pm 0.2$) for 44 days and the pH was kept constant
153 by replacing the phosphoric acid solution based on predetermined intervals. Specifically, the
154 solution was replaced every day during the first 7 days and every second day after that until 14
155 days of immersion. From 14 days, it was renewed every three days until the end of the acid
156 immersion (44 days). The solid surface/liquid volume was approximately 0.29 cm^{-1} and
157 solid/liquid volume ratio was 0.20 throughout the immersion period. The pH level was selected
158 based on the scenarios where concrete structures are applied in sewage wastewater pipes, food
159 process or mining industries [48-50]. The top and bottom surfaces of the specimens were sealed
160 using inert silica gel to ensure a horizontal direction of acid ingress and the corresponding
161 experimental setup can be referred to the literature [8]. Another batch of specimens were

162 submerged in distilled water as a reference which was also regularly replaced with the same
163 renewal frequency as the phosphoric acid solution. In order to quantify the alkalinity of pore
164 solutions of the three binder mixes, the continuous pH changes over the first day of immersion
165 before renewal of acid or water were monitored using HI 3222 pH/ORP/ISE meter with an
166 accuracy of 0.01. This measurement was only conducted within one day of immersion because
167 the greatest pH changes occur within one-day of immersion [35, 51]. It is worth pointing out
168 that unless further introductions, this exposure regime applies to the samples for all
169 measurements

170 2.3.3. Degradation kinetic measurements

171 *Degradation depth*

172 Total degradation depth (TDD), simplified as degradation depth was used as the direct
173 indicator of degradation kinetics which is a numerical combination of dissolved/detached depth
174 (DD) [16] due to partial dissolution and/or detachment of specimens in acid solution and
175 apparent degradation depth (ADD) as indicated by phenolphthalein colouration method. A
176 presentation of the TDD, DD and ADD after the spray of phenolphthalein solution is shown in
177 Fig. 2. This method, based on DIN EN 14630:2007-01, has been widely used as a reliable
178 indicator of various degradation processes [36, 52-55]. The detailed description of the
179 degradation depth measurement is introduced in the following references [8, 24]. The
180 measurements were conducted on small disks cut from 6 parallel specimens which were
181 continuously submerged in the acid solution throughout the entire immersion period.



183 **Fig. 2.** An image of a disk-shaped sample cross-section after phenolphthalein spray showing the
184 determination of total degradation depth (TDD), ADD and DD.

185 *Mass changes*

186 Mass changes were examined before each measurement of degradation depth. At each
187 sampling stage, specimens were taken out from the phosphoric acid solution gently and dried
188 slightly using a wet cloth before weighing to remove surface water. The whole weighing
189 process was completed within 30 seconds to minimize the water evaporation from sample
190 surfaces using a digital scale with a precision of ± 0.01 g. Samples were then positioned back
191 into the phosphoric acid solutions. At the same time, mass changes of the references submerged
192 in distilled water were also recorded.

193 *Leaching rates of related ions*

194 Concentrations of different elements including Ca, Na, Al and Si in the phosphoric acid
195 solution were analysed by Inductively coupled plasma-optical emission spectrometer (ICP-
196 OES) analyser (Optima 4400, Perkin Elmer, USA). Three cylindrical samples (Φ 27.5 mm \times
197 H 55 mm with volume of 32.65 cm³) of each mix was immersed in 900 mL phosphoric acid
198 solution separately with the same pH level (2.0 ± 0.2). The solid/liquid volume ratio was 0.11
199 for all mixes because a higher ratio could lead to the concentrations of ions above the testing
200 limits. The renewal of acid occurred right after 3, another 4 (7 days in total), another 3 (10 days
201 in total), and another 4 (14 days in total) days of immersion, the frequency of which was lower
202 than that of the degradation depth measurements because of a smaller solid/liquid volume ratio
203 used in this test. The concentrations of Ca, Na, Al, Si, released out from the specimens in the
204 corresponding leachate phosphoric acid solutions were measured right before each renewal of
205 acid, namely after a total of 3, 7, 10 and 14 days as well as 21 days by the end of the immersion.

206 **2.3.4. Mineralogical, chemical and microstructural analysis**

207 Mineralogical and chemical characteristics of both degraded and undegraded part of
208 specimens were evaluated using X-ray diffraction analysis (XRD), thermogravimetric analysis
209 (TGA), derivative thermogravimetry (DTG) and environmental scanning electron microscope
210 equipped with energy dispersive X-ray spectroscopy (ESEM/EDS). Micro X-ray computed
211 tomography (μ -XCT) was also used to provide non-destructive three-dimensional (3D)
212 microstructural information on the degraded and undegraded regions of the specimens.

213 Crushed samples from both degraded and undegraded parts of the specimens after 44-day
214 immersion were grounded into fine powders (passing through the 75 μ m sieve (No.200))
215 followed by drying in a desiccator for 24 hours at room temperature prior to XRD and

216 TGA/DTG tests. For ESEM/EDS, samples after 14-day immersion were first pre-heated at 60
217 °C for 48 hours to expel all moisture and then sectioned including both degraded and
218 undegraded part, impregnated with epoxy resin and polished using SiC abrasive paper prior to
219 the analysis. The 3D microstructures of a piece of specimens cut off from the sample surface
220 after 21-day immersion were examined using XCT. The dimension of each binder mix was
221 around 1 mm in width and length to obtain a high resolution (1.77 μm). The 14-day and 21-
222 day testing point was selected because the degradation performance is discernible enough after
223 these immersion periods, shortly after the induction stage for the 50Slag_50FA sample.

224 XRD patterns were recorded using a Bruker D8 Advance diffractometer with Cu – $K\alpha$
225 radiation and data were collected in a 2θ range of 10-70°. The scanning rate was 1.2°/min.
226 TGA/DTG was carried out in a PerkinElmer Diamond instrument. ESEM was conducted using
227 an FEI Quanta instrument with a 15 kV accelerating voltage and the working distance was 10
228 mm. EDS was run by a Link-Isis (Oxford Instruments) X-ray energy dispersive detector for
229 chemical composition analysis. Micro-CT analysis was performed with a Phoenix Nanotom m
230 (Waygate Technologies) operated using xs control and Phoenix datos|x acquisition
231 reconstruction software (both Waygate Technologies). Micro-CT scans were collected over
232 47.5 minutes using an x-ray energy of 60 kV and 240 μA collecting 1400 x-ray projections
233 through a full 360 degrees of rotation. Reconstructed data was exported in a 16-bit format and
234 imported to Avizo (Thermo Fisher Scientific) for analysis.

235 **2.3.5. Intrinsic acid resistance measurement**

236 In order to eliminate the influence of porous structure on the acid resistance of different
237 cementitious binders, specimens were ground to fine powders (size < 90 μm). Then they were
238 immersed in a nitric acid solution (approximately 0.06 wt.%, pH = 2.0 \pm 0.2) to avoid possible
239 clogging effect that may happen to other acids because nitrates are highly soluble without any
240 precipitation [56]. For each mix, 0.2 g powders were firstly immersed in 200 mL nitric acid
241 solution and then constantly stirred for one minute followed by natural deposition in ambient
242 environment. This small amount of powder but large volume of acid solution was employed to
243 avoid the need for acid renewal due to pH changes. After 48-hour immersion, three suspension
244 solutions for different mixes were vacuum filtered by gravity filter paper (8 μm in pore size).
245 The powders on the filter paper were then rinsed with deionised water completely until a neutral
246 pH was obtained. After that, the insoluble residue powders were dried at 50 °C for at least 3
247 days to remove any moisture until a constant mass was achieved. Finally, the residue powder
248 was weighed to calculate the dissolution rate (DR) using the following equation:

249

$$DR = \frac{M_{\text{before}} - M_{\text{after}}}{M_{\text{before}}} \quad (1)$$

250 where M_{before} and M_{after} refers to the mass before immersion and the dry mass of residual
251 powders respectively. In this study, M_{before} is approximately 0.2 g for all binder mixes. The
252 measurement was repeated twice.

253 Since the dissolution rate is highly dependent on the surface area of reactants [57], the
254 surface area of the initial powdered sample after 56 days of curing was also quantified by
255 performing Brunauer-Emmett-Teller (BET) analysis in compliance with ISO 9277 [58].
256 Powdered samples were first preconditioned by outgassing, drying under vacuum at 150 °C for
257 24 hours [59]. Then their surface areas were analysed using nitrogen absorption/desorption
258 method [60]. It is worth mentioning that the small amount of samples (around 0.2 g) but higher
259 volume of nitric acid solution used could minimise the possible neutralisation effect of
260 powdered samples.

261 **3. Results and discussion**

262 **3.1. Basic properties before acid immersion**

263 The basic properties of the three mixes prior to the acid exposure are shown in Table 3. From
264 Table 3, it is clear that all specimens obtained similar compressive strength (62 ± 3 MPa) before
265 immersion. 65Slag_35OPC and 50Slag_50FA had the highest and lowest water absorption and
266 VPV respectively, due to their largest and lowest amount of mixing water used (Table 2)
267 accordingly. However, 65Slag_35OPC pastes displayed the lowest capillary sorptivity despite
268 of its highest water absorption and VPV. This might be explained by considering its porous
269 structure changes during the 56-day curing period. Due to the largest amount of mixing water
270 used, many pores were left in the binder matrix after water evaporation, leading to the highest
271 water absorption and VPV [2]. However, the late hydration process of this paste due to partial
272 replacement of OPC by GGBFS refined its porous structures [61], leading to the formation of
273 many isolated pores which reduced the continuity of pore structures. Thus, a low capillary
274 sorptivity was obtained. As a higher rate of water ingress caused by capillary forces indicates
275 a higher susceptibility of early-stage acid attacks as water is the vehicle of aggressive ions, it
276 suggests that 50Slag_50FA and 100OPC are more vulnerable towards acid attacks compared
277 to 65Slag_35OPC from the perspective of porous media [2].

278 **Table 3**

279 Basic properties of the paste samples used in this test prior to the immersion in the phosphoric
280 acid attack.

Sample ID	Water absorption (%)	VPV (%)	Capillary sorptivity (mm/min ^{0.5})	Compressive strength (MPa)
50Slag_50FA	17.7 ± 0.1	29.3 ± 0.2	0.36 ± 0.03	64.33 ± 5.78
65Slag_35OPC	26.6 ± 0.1	38.4 ± 0.1	0.14 ± 0.05	59.90 ± 6.44
100OPC	19.6 ± 0.3	31.3 ± 0.4	0.33 ± 0.01	64.92 ± 3.78

281 VPV-Volume of permeable voids.

282 3.2. Degradation kinetics

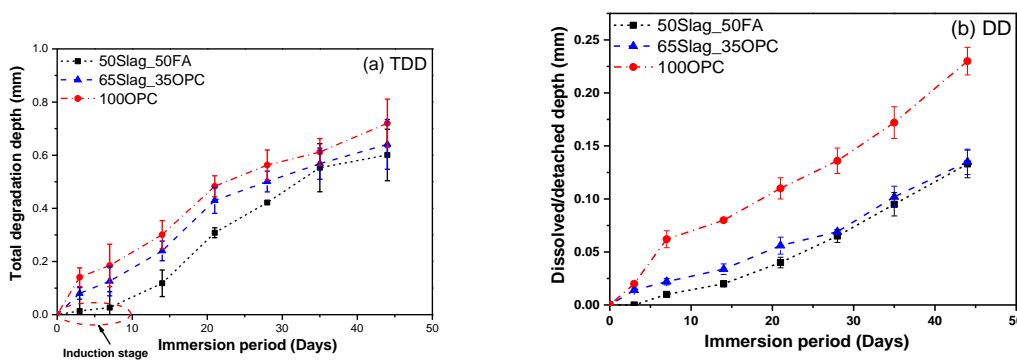
283 3.2.1. Degradation depth

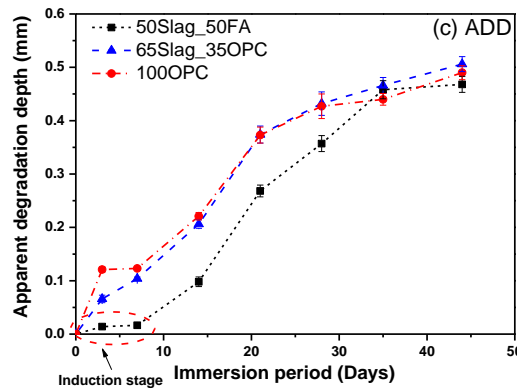
284 The degradation depths, including TDD, DD and ADD of all mixes exposed to the
285 phosphoric acid solution within 44 days of immersion are shown in Fig. 3(a)-(c). From Fig.
286 3(a), the TDD of 50Slag_50FA specimen was less than that of the two OPC-based counterparts
287 throughout the immersion period, especially within about 0-14 days. Besides, it seems that
288 50Slag_50FA specimen displayed an induction stage within 7 days of immersion with very
289 little degradation depth measured as highlighted in a red dash circle. After 7 days, the TDD of
290 50Slag_50FA increased considerably until 35 days followed by a lower rate of increase until
291 the end of the 44-day immersion with final TDD at 0.60 mm. In contrast, the 65Slag_35OPC
292 had an almost linear increase in TDD first within 21 days and then the TDD increased at a
293 lower rate until the end of exposure. 100OPC followed a similar trend as that of 65Slag_35OPC
294 but with larger TDD throughout the whole immersion period. After 44 days of immersion, the
295 TDD of 65Slag_35OPC and 100OPC was 0.64 and 0.72 mm respectively.

296 For DD values (Fig. 3(b)), 50Slag_50FA and 65Slag_35OPC specimens exhibited similar
297 trends, increasing almost linearly against immersion period with the DD of 65Slag_35OPC
298 slightly larger. In comparison, 100OPC had a much larger DD over the entire immersion period
299 compared to the other two binders. This significant difference can be explained by considering
300 the different intrinsic chemical stability of main components in the binder matrix: portlandite
301 [Ca(OH)₂], ettringite and C-S-H gel (the main hydration products in 100OPC binder) can be
302 dissolved and/or decomposed completely by acid attacks via decalcification process when pH
303 is around 3 or lower regardless of acid types [62]. As C-S-H gel is the main contributor to the
304 strength of OPC-based binders [63], accounting for 60%-75% of the total volume of paste [64,
305 65], its dissolution and decomposition can thus result in almost complete disintegration of the
306 whole binder matrix (evidenced by the largest DD). However, due to higher contents of Al but
307 lower contents of Ca in GGBFS and FA compared to OPC (Table 1), the binding gels formed
308 in 50Slag_50FA or 65Slag_35OPC have more Al and less Ca compared to 100OPC. It is
309 confirmed that gels with more Al are more stable and resistant towards decalcification due to

310 their more intensely cross-linked networks [66]. Besides, Al and Si have a higher pH stability,
 311 or greater ability to not leach out of binder at a certain pH, compared to Ca [54]. These explain
 312 why 50Slag_50FA and 65Slag_35OPC obtained much less DD compared to 100OPC.

313 From Fig. 3(c), 50Slag_50FA had very little ADD within the 7 days of immersion (also
 314 marked as ‘induction stage’) followed by a significant rise from 7-35 days. 65Slag_35OPC and
 315 100OPC samples obtained similar ADD values with a seemingly proportional increase over
 316 the immersion period. After 44 days, the ADD was 0.47, 0.51 and 0.49 mm for 50Slag_50FA,
 317 65Slag_35OPC and 100OPC respectively. Different ADD are closely associated with available
 318 OH⁻ (hydroxyls) in the binder matrix based on its definition: if the pore solution of binder
 319 matrix has a high concentration of OH⁻ that can neutralise H₃O⁺ from the acid solution, the pH
 320 of the pore solution can maintain relatively stable for a certain period. However, if the
 321 concentration of OH⁻ is not high enough to neutralise H₃O⁺ or they are neutralised at the
 322 expense of the formation of many cracks near the sample surface, the pH of the pore solution
 323 would decrease rapidly. Hence, the delayed ADD evolution of 50Slag_50FA evidenced by the
 324 induction stage suggests it has a large reservoir of soluble and mobile alkalis which prevent a
 325 sudden drop in the pH of AASF pore solutions [67]. In comparison, the instant response of pH
 326 increment implies that the two OPC pastes either had a lower concentration of OH⁻ in the pore
 327 solution and/or the binder matrix was severely disintegrated, thus providing almost no extra
 328 ‘protection’ against the acid penetration.



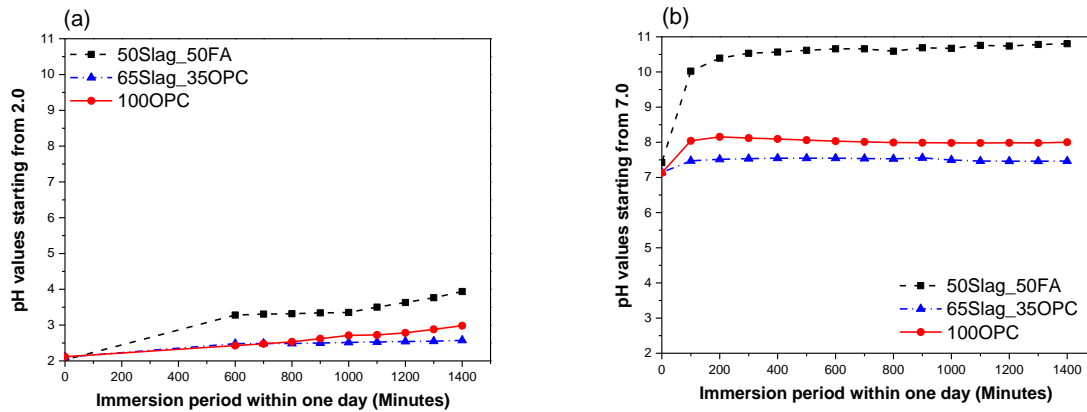


330

331 **Fig. 3.** The (a) TDD, (b) DD and (c) ADD of the three cementitious pastes exposed to the phosphoric
 332 acid ($\text{pH} = 2.0 \pm 0.2$) over 44-day of immersion.

333 To confirm this, the pH evolutions over the first day of immersion in phosphoric acid and
 334 water are shown in Fig. 4. It is apparent that 50Slag_50FA led to a greater increase in the pH
 335 of the corresponding solutions compared to that of the OPC-based peers both in the phosphoric
 336 acid and in water, suggesting that it has a stronger neutralisation capacity. Considering the least
 337 ADD of 50Slag_50FA, it seems to have an ability to maintain the pH of pore solution at a high
 338 level ($\text{pH} > 8.3$) because of a large reservoir of OH^- that is readily available to neutralise
 339 external H_3O^+ ions. This result corresponds well with the other studies [51, 67] which reported
 340 that the concentration of OH^- in the pore solution of one type AASF with the same slag/FA
 341 ratio is more than 1000 mmol/L, indicating a pH higher than 14. Besides, bound alkalis provide
 342 the AAMs with a large reservoir of exchangeable cations to prevent a sharp drop in the pH of
 343 pore solutions. However, the pH of the pore solutions of OPC binders is relatively lower,
 344 ranging between 12.5 and 13.5 [68-70] and that's why OPC-based binders had larger ADD
 345 than that of the 50Slag_50FA paste. The significant increase in the ADD of 50Slag_50FA after
 346 7 days reveals that most of the OH^- available were almost consumed. The final slightly larger
 347 ADD for 65Slag_35OPC than 100OPC is consistent with the former's smaller increase in the
 348 pH in Fig. 4(a) and (b). This is because 100OPC has a large amount of Portlandite which is
 349 able to consume H_3O^+ , also known as the buffer effect [71].

350 In conclusion, the 'induction stage' in ADD and TDD is closely associated with the higher
 351 neutralisation capacity of the 50Slag_50FA specimen, providing a buffering effect during the
 352 early stage.



353

354 **Fig. 4.** The pH variations of (a) phosphoric acid solution and (b) water solution within the first day of
 355 immersion.

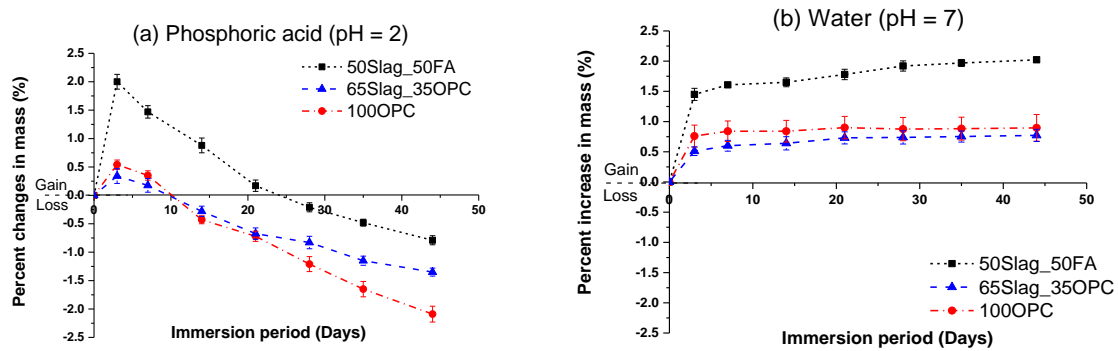
356 3.2.2. Mass changes

357 Fig. 5 presents the mass changes of the three binder mixes in the phosphoric acid and in
 358 water as reference over the early-stage immersion period. The obvious initial mass gain for all
 359 binder mixes regardless of phosphoric acid solution or water is due to water absorption and
 360 similar results were also reported in previous studies [72, 73]. After a certain period, mass
 361 losses were observed for specimens exposed to phosphoric acid whereas a slight mass increase
 362 or a constant mass was observed for 50Slag_50FA and OPC-based binders respectively for the
 363 immersion in water.

364 For immersion in the phosphoric acid, 50Slag_50FA experienced the largest mass increase
 365 (2%) after about three days followed by a decrease in mass gain up to about 24 days. After that,
 366 the actual mass loss occurred with the final mass loss at 0.79% by end of the immersion. The
 367 largest mass increase for 65Slag_35OPC and 100OPC sample was 0.34% and 0.54%
 368 respectively after 3-day immersion, much smaller than that of the 50Slag_50FA. An apparent
 369 mass loss compared to the initial value was observed after about 10 days for the two OPC-
 370 based mixes, about 14 days earlier compared to the 50Slag_50FA. The highest mass gain and
 371 delayed mass loss for the 50Slag_50FA might be associated with its highest capillary sorptivity
 372 (Table 3), relatively stability of binding components and possible precipitations of some
 373 reaction products. For 65Slag_35OPC sample, the mass loss decelerated gradually whereas the
 374 mass loss decreased almost constantly for 100OPC. The final mass loss of the two was 1.35%
 375 (65Slag_35OPC) and 2.09% (100OPC).

376 In conclusion, the mass losses of the three mixes were consistent with the degradation
 377 depths, with an increasing order at 50Slag_50FA < 65Slag_35OPC < 100OPC. It is worth
 378 noting that the much greater mass gain owing to acid solution ingress for the 50Slag_50FA but

379 similar starting point of the loss in mass gain at about 3 days for all mixes suggest that this
 380 binder is more resistant towards mass losses due to this acid attack compared to the OPC-based
 381 peers. It is suggested to use fully-saturated specimens before immersion in acid solutions to
 382 avoid misleading mass gains caused by the ingress of acid solutions.



383
 384 **Fig. 5.** Mass changes over 44-day immersion time for the three binder mixes in (a) phosphoric acid
 385 and (b) water.

386 3.2.3. Leaching rates of related elements

387 The leaching behaviour the related elements released from the three mixes during 21 days
 388 of immersion in the phosphoric acid and in water are depicted in Fig. 6. The cumulative
 389 concentration of Na, Ca, Al and Si is denoted as [Na], [Ca], [Al] and [Si] respectively hereafter.
 390 Due to insignificant contents of Na in the OPC-based binders, [Na] is not discussed for OPC-
 391 based binders.

392 During immersion in the phosphoric acid, a remarkable increase in [Ca] can be observed for
 393 all mixes compared to the [Si], [Al] or [Na]. For instance, the [Ca] was 1606.6 ppm for the
 394 solution containing 50Slag_50FA, which was even higher than the total sum of [Si], [Al] and
 395 [Na] (1172.7 ppm). This phenomenon is attributed to the high content of Ca in all mixes and
 396 higher neutralisation capacity of bivalent Ca^{2+} ions compared to monovalent Na^+ .
 397 50Slag_50FA also led to a large [Na] which was 883.4 ppm owing to the sodium-based alkaline
 398 activator used while making the specimen. The high [Ca] and [Na] are in line with the highest
 399 neutralisation capacity and the presence of 'induction stage' for 50Slag_50FA because these
 400 counter-balancing ions are accompanied with a lot of OH^- , maintaining the pH value of the
 401 pore solution for a while without considerably affecting the stability of the binding phase. The
 402 [Al] and [Si] for 50Slag_50FA were much lower, which was 14.8 ppm and 274.5 ppm
 403 respectively. Similarly, the corresponding value was 22.1 and 309.0 ppm for 65Slag_35OPC,
 404 5.4 and 208.5 ppm for 100OPC respectively. All of these suggest that Al and Si are less
 405 sensitive compared to Ca when exposed to the acid attack [54]. It is worth noting that for all

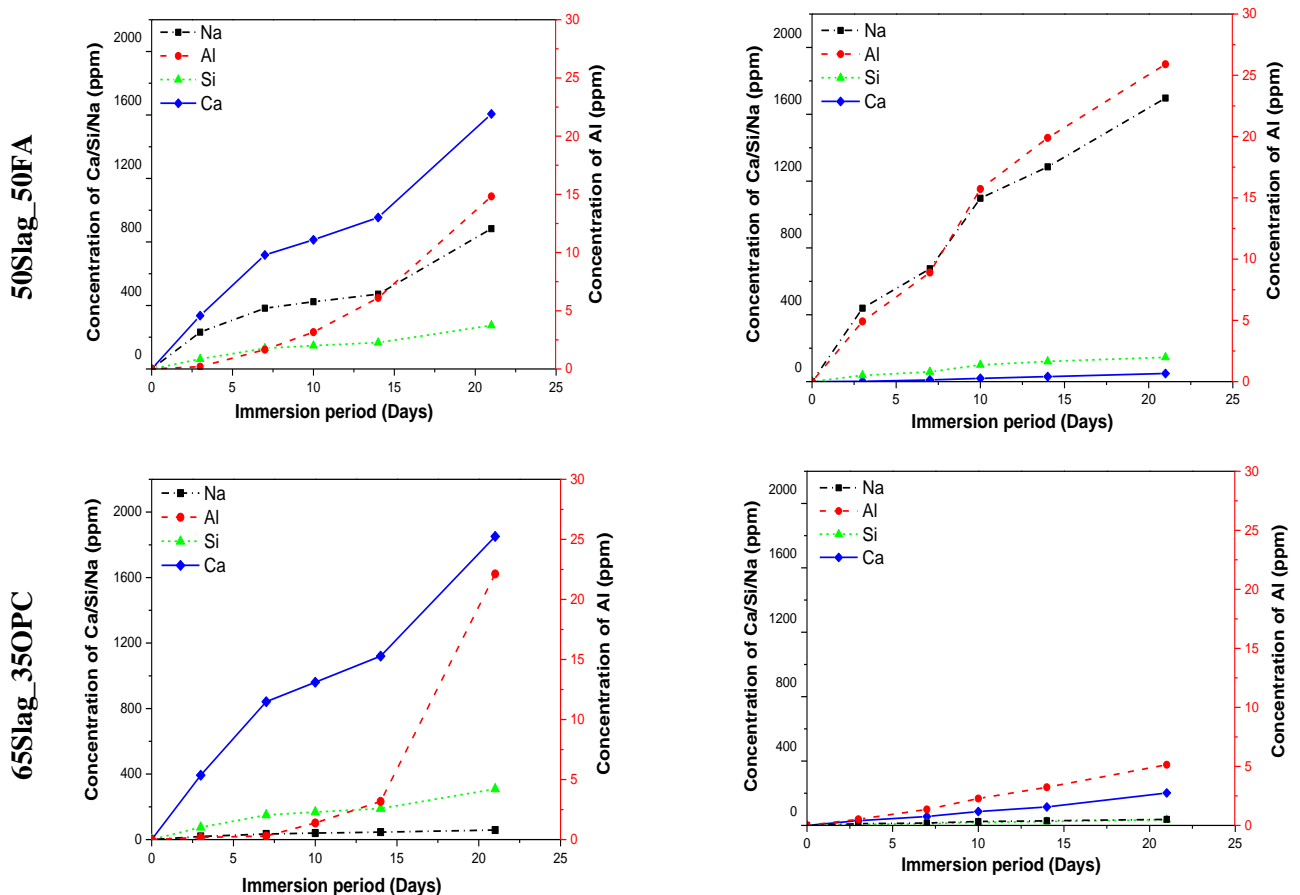
406 mixes, the release of Al seemed to be curbed probably because of the relative high stability of
 407 Al-bearing phases, such as C-(N)-A-S-H in the 50Slag_50FA and calcium aluminate phases in
 408 OPC-based binders [19, 74].

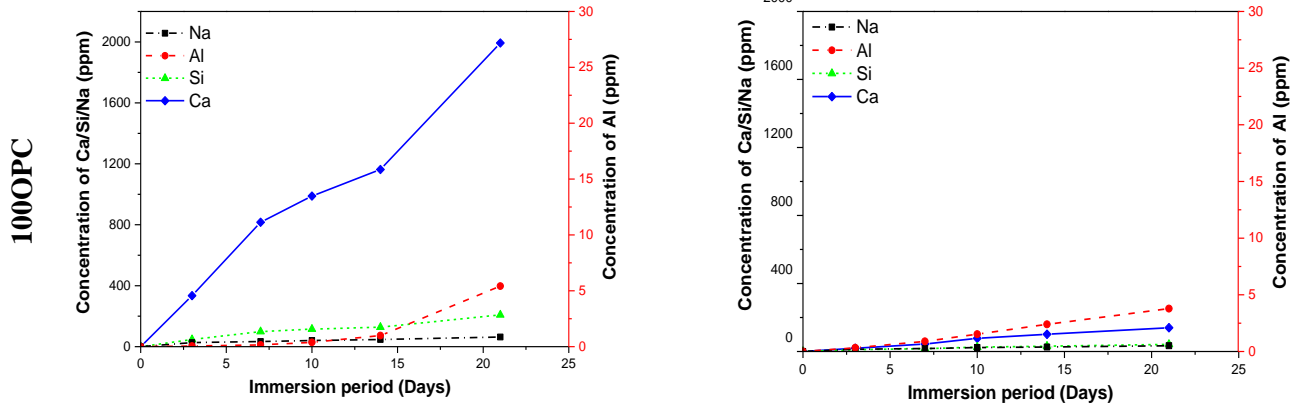
409 Compared to the [Ca] in the phosphoric acid, [Ca] in water was much lower irrespective of
 410 binder mixes indicating that Ca is quite sensitive to H_3O^+ induced by the acid solution. In
 411 addition, the [Na] and [Al] in water for 50Slag_50FA was higher due to their high mobility,
 412 especially for Na. The OPC-based two mixed binders had similar [Al] and [Si] which increased
 413 almost linearly with an increase in the immersion periods.

414 In summary, Ca is much more sensitive towards H_3O^+ compared to Si and Al, corresponding
 415 well with the results from other research [75, 76]. Moreover, apart from Ca, 50Slag_50FA can
 416 release a large amount of Na which plays an important role in consuming H_3O^+ ions produced
 417 by acid solutions and maintaining a stable pH of the pore solution.

(a) Phosphoric acid

(b) Water





418

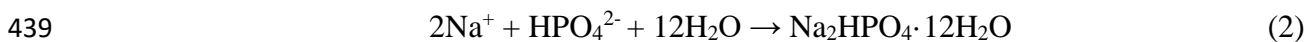
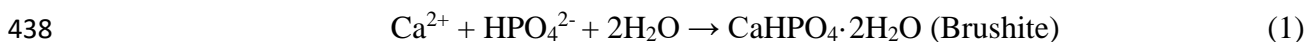
419 **Fig. 6.** Cumulative concentrations of different elements in the two solutions released from the three
 420 mixes within 21 days of immersion, (a) Phosphoric acid; (b) Water.

421 3.3. Microstructural characterisation

422 3.3.1. Mineralogy

423 *X-ray diffraction (XRD)*

424 Fig. 7 shows the XRD spectra of the three mixes after 44 days of immersion in the phosphoric
 425 acid solution. Based on Fig. 7(a), it can be seen that due to the acid attack, major components
 426 such as Ca-bearing gismondine ($\text{CaO} \cdot \text{Al}_2\text{O}_3 \cdot 2\text{SiO}_2 \cdot 4\text{H}_2\text{O}$ PDF # 00-002-0096) and C-(N)-(A)-
 427 S-H (a type of calcium silicate hydrate substituted by Al and Na) [39, 77-79] which are present
 428 in the undegraded part of 50Sslag_50FA all disappear. Quartz (PDF # 00-001-0649) and mullite
 429 (PDF # 00-001-0613), however, still appear due to some unreacted FA in the degraded part.
 430 This result implies that the phosphoric acid attack resulted in decalcification of the main
 431 binding gels in the 50Sslag_50FA paste along with dealkalisation and dealumination. The
 432 dealkalisation and dealumination were also verified by the leaching results of Al and Na in Fig.
 433 6. Moreover, some phosphates were identified in the degraded part, such as Brushite
 434 ($\text{CaHPO}_4 \cdot 2\text{H}_2\text{O}$ PDF # 00-001-0395) and sodium phosphate hydrate oxide ($\text{Na}_2\text{HPO}_4 \cdot 12\text{H}_2\text{O}$
 435 PDF # 00-001-0223). The formation of Brushite was also reported in another study [1] due to
 436 silage effluent attacks as silage effluents also contain phosphates. Possible chemical reactions
 437 are shown below:

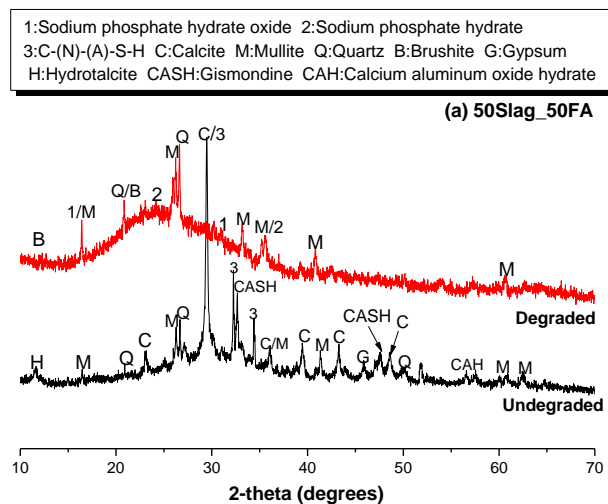


440 Fig. 7(b) and (c) shows that Portlandite ($\text{Ca}(\text{OH})_2$ PDF # 00-001-1079), C-S-H gel (PDF #
 441 00-002-0068), calcite (CaCO_3 PDF # 00-001-0837) and ettringite ($\text{Ca}_6\text{Al}_2(\text{SO}_4)_3(\text{OH})_{12} \cdot 26\text{H}_2\text{O}$
 442 PDF # 00-002-0059) are main phases in the OPC-based binding matrix without acid attacks.

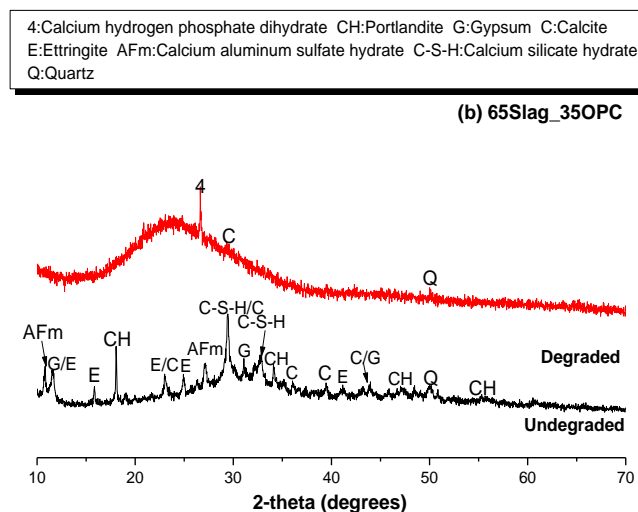
443 However, all of these phases disappear in the corresponding degraded parts, indicating their
 444 vulnerability to the phosphoric acid [74]. For 65Slag_35OPC, minor traces of quartz (PDF #
 445 00-001-0649) and calcium hydrogen phosphate dihydrate ($\text{CaHPO}_4 \cdot 2\text{H}_2\text{O}$ PDF # 00-001-0653)
 446 were detected in the degraded part. Brushite ($\text{CaHPO}_4 \cdot 2\text{H}_2\text{O}$ PDF # 00-001-0395) and a type
 447 of calcium phosphate hydrate ($\text{Ca}(\text{H}_2\text{PO}_4)_2 \cdot \text{H}_2\text{O}$ PDF # 00-001-0471) can be observed in the
 448 degraded part of 100OPC binder. The presence of the $\text{Ca}(\text{H}_2\text{PO}_4)_2 \cdot \text{H}_2\text{O}$ can be explained by
 449 the reaction below that could happen in the interstitial solution or at the surface of the sample:



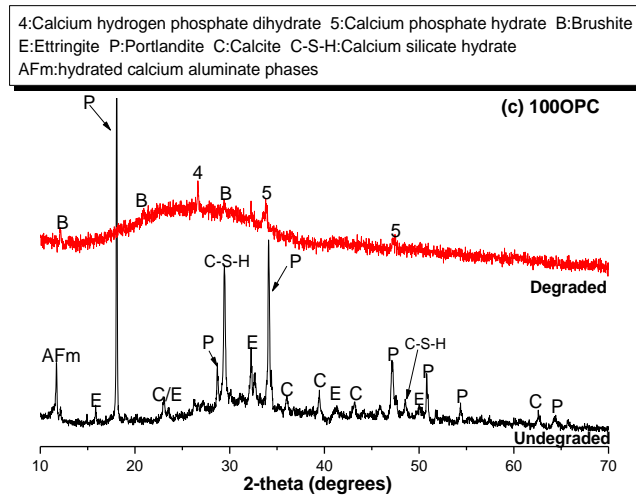
451 It is also noticed that after the phosphoric acid immersion, a wide halo is present in degraded
 452 parts of all mixes (extending from around 15 to about $35^\circ 2\theta$). These can be ascribed to the
 453 formation of amorphous phases due to acid attacks [19]. The wider and more flattened halo of
 454 100OPC sample than the other two binders indicates a more severely degraded part, consistent
 455 with the highest degradation kinetic of 100OPC.



456



457



458

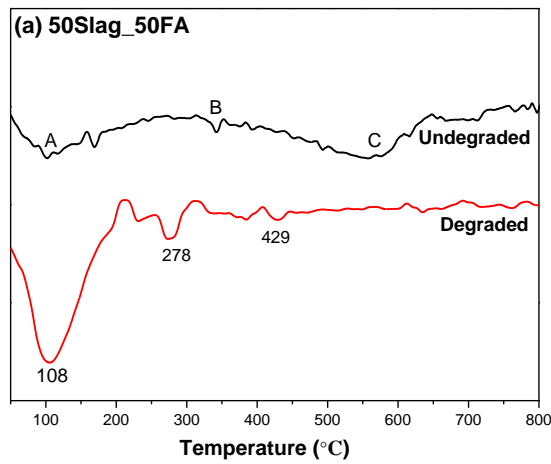
459 **Fig. 7.** XRD patterns of the three mixture pastes (a) 50Slag_50FA; (b) 65Slag_35OPC and (c)
 460 100OPC including both degraded and undegraded parts after 44-day immersion period in the
 461 phosphoric acid ($\text{pH} = 2.0 \pm 0.2$).
 462

462 **Differential Thermogravimetry (DTG)**

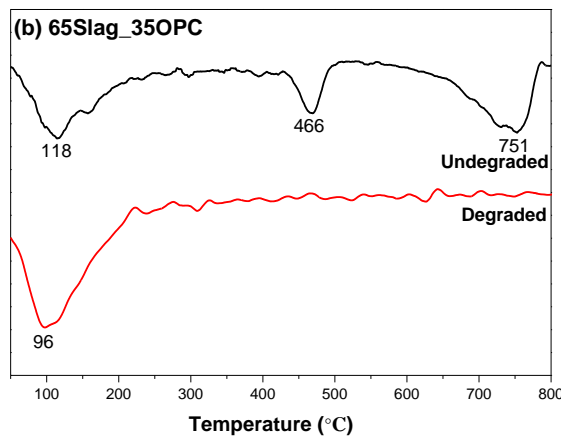
463 DTG curves of the three binder mixes including degraded and undegraded part of specimens
 464 are shown in Fig. 8. Table 4 lists the characteristic peak attributions for all the curves. It can be
 465 observed that there are three small peaks marked as 'A', 'B' and 'C', belonging to evaporable
 466 water or moisture loss from 50Slag_50FA undegraded binding matrix [80-82], decomposition
 467 of C-A-S-H and C-A-H [83-85] and decomposition of carbonates (e.g. calcite) [86, 87],
 468 respectively. In comparison, no 'B' and 'C' peaks could be observed in the degraded part.
 469 Rather, two obvious peaks located at 278 and 429 °C are present which might be associated
 470 with the formation of calcium phosphates, as verified in XRD patterns. Besides, a significant
 471 mass loss exists at around 108 °C, indicating that more water (loosely bound or unbound) is
 472 evaporable after the acid attack due to the transformation of many original crystalline phases
 473 to amorphous ones, as shown in Fig. 7(a).

474 For the undegraded part of the OPC-based binders, the first mass occurring at 118 °C and
 475 117 °C respectively for 65Slag_35OPC and 100OPC can be assigned to the loss of evaporable
 476 free water, dehydration of C-S-H gel and ettringite [80, 81, 88]. The peaks centered at 466 and
 477 467 °C for 65Slag_35OPC and 100OPC respectively are due to the dehydroxylation of
 478 Portlandite [81]. The last significant mass loss located at around 750 or 751 °C is attributed to
 479 the decomposition of carbonate minerals, such as calcite [89, 90], in accordance with the XRD
 480 results. Similar to XRD, corresponding peaks assigned to Portlandite and calcites are not
 481 present in the DTG curves of the degraded part. The only obvious mass loss located at lower
 482 temperatures, 96 °C (65Slag_35OPC) and 94 °C (100OPC), compared to those in the

483 undegraded part, indicates the presence of a larger amount of less tightly bound water. This is
484 in large part due to the formation of some less crystalline and amorphous phases such as silica-
485 gel after the phosphoric acid immersion, corresponding well with the wide halo in the XRD
486 results. It is noteworthy that no phosphates are noticeable in OPC-based DTG curves, probably
487 because the total amount of these phosphates are too small to be detected or most of them were
488 dissolved in the acid solution. Based on the XRD results which show traces of calcium
489 phosphates, it is highly possible only a little amount phosphates were left in the degraded layer
490 of OPC binders.

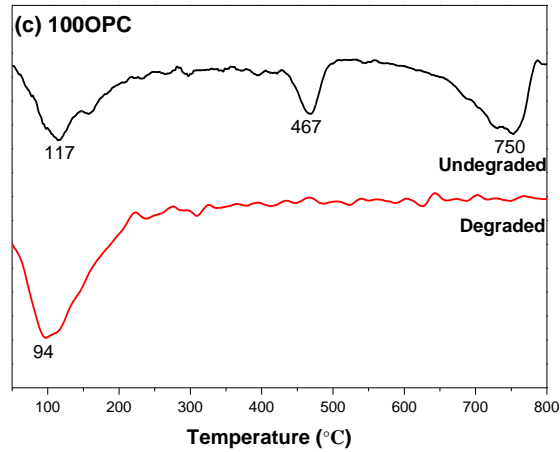


491



492

493



494

495 **Fig. 8.** DTG curves of the three mixes including degraded and undegraded part of the specimen.

496 **Table 4**

497 Temperature ranges within or at which corresponding changes in phases take place.

Different phases and changes	Temperature ranges (°C)	References
Loss of evaporable water	0–120, usually < 100	[80, 81]
Removal of the moisture within C-S-H type gel	50-200	[91, 92]
Loss of water in N-A-S-H	≈ 100	[82]
Loss of bound water in C-(A)-S-H	30-650	[91]
Decomposition of ettringite	114-116/110-170/104-114	[93, 94]/[81]/[95]
Mass loss of AFm phases	146	[96-99]
Dehydroxylation of calcium hydroxide	450-550/430-520	[81, 95, 100]/[86]
Decomposition of carbonates	560-700/741-797	[86, 87]/[89, 90]

498

499 3.3.2. Microstructure

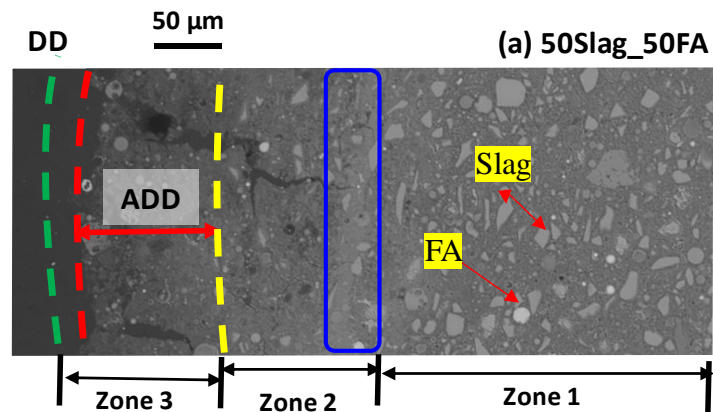
500 *ESEM and EDS*

501 SEM images in backscattering mode and elemental distributions of the three mixes after 14
 502 days of immersion are shown in Fig. 9 and Fig. 10 respectively. The corresponding DD and
 503 ADD obtained from Fig. 3 are also marked. The DD of the 50Slag_50FA, 65Slag_35OPC and

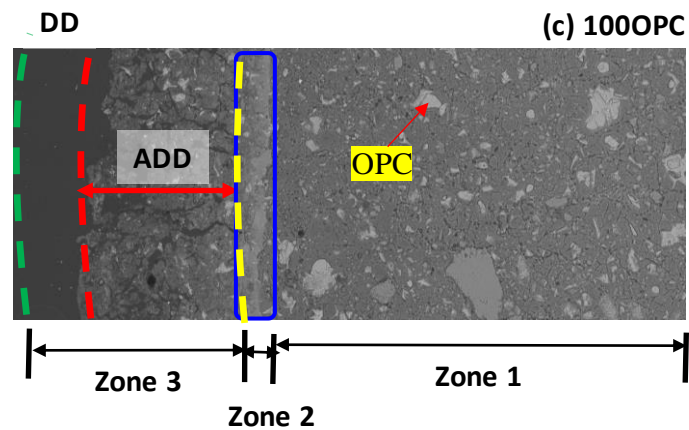
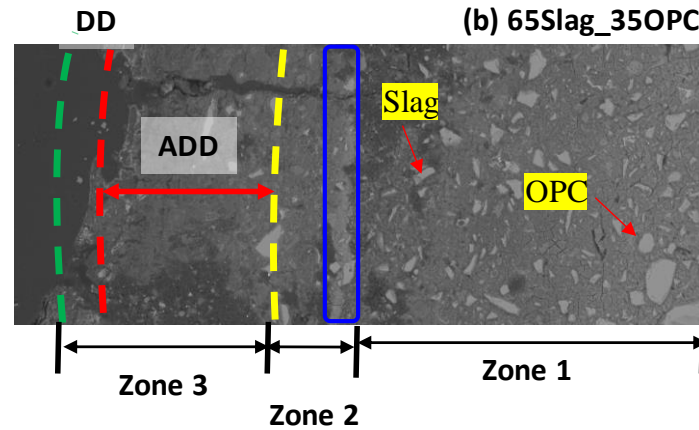
504 100OPC was 20.0, 33.8 and 80.0 μm respectively and the corresponding ADD was 96.6, 206.2
505 and 188.4 μm respectively.

506 In Fig. 9, it is clear that three zones can be identified for all the samples: Zone 1 represents
507 the undegraded part of the samples with brighter grey colour compared to other regions as it
508 contains many unhydrated OPC particles for OPC-based binders or unreacted GGBFS and FA
509 particles for 50Slag_50FA [72, 101]. Zone 2 is a transition zone starting from a bright grey
510 narrow strip (partitioned as blue solid line frames) which should be a region rich in phosphates
511 (as discussed later) to the right boundary of ADD (yellow dashed line, also considered as the
512 'reaction front'). In this zone, both obvious cracks (closer to surface) and unreacted/unhydrated
513 particles exist. Zone 3 is composed of DD and ADD with many microcracks and voids,
514 indicating a severe degradation result.

515 The most distinct part is Zone 2 of 50Slag_50FA compared to that of the other OPC-based
516 pastes. Firstly, the width of the narrow strip is apparently larger indicating more precipitations
517 of phosphates, in accordance with the mineralogical analysis (shown in Fig. 8(a)). Additionally,
518 50Slag_50FA has a thicker Zone 2, implying a stronger resistance to the ingress of H_3O^+ ions
519 as they need to penetrate this zone first before attacking new undegraded areas. This is critical
520 for maintaining high resistance towards acid attacks. This thicker zone 2 has also been reported
521 in previous studies [19, 102].



522



523

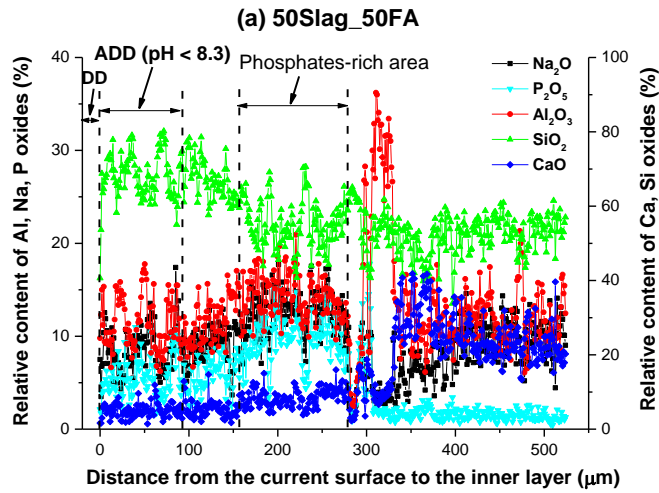
524

525 **Fig. 9.** SEM images of the paste samples (a) 50Slag_50FA; (b) 65Slag_35OPC and (c) 100OPC after
 526 14 days of immersion in the phosphoric acid.

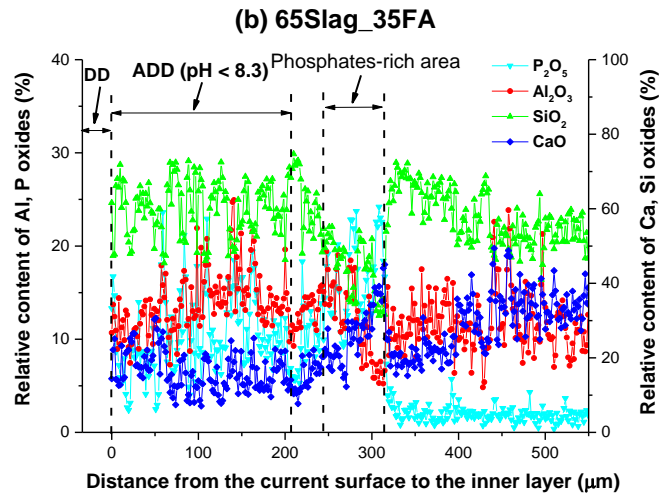
527 The elemental distributions from the surface to the inner part of the specimens are shown in
 528 Fig. 10. Consistent with the locations of the blue solid line frames in Fig. 9, a much higher
 529 phosphorus concentration is observable implying the precipitations of different phosphates. A
 530 closer examination shows that the phosphates-rich area of 50Slag_50FA is located farther from
 531 the reaction front followed by that of 65Slag_35OPC and 100OPC. For all mixes, the relative
 532 concentration of Ca decreased as approaching to the degraded surface while Al and Si
 533 displayed the opposite trend, in agreement with the leaching behaviour of these elements,
 534 which demonstrates that Ca is more sensitive towards acid attacks compared to Al and Si.

535 50Slag_50FA encountered an increase in the relative concentration of Al accompanied with
 536 a decrease in the Ca and Na relative content. This can be explained by the ease of ion exchanges
 537 of Ca and Na with H_3O^+ compared to Al, in line with the delayed leaching behaviour of Al as
 538 shown in the ICP-OES analysis and other studies [103]. It seems that Al is much less mobile
 539 in AAM binding gels because according the previous studies, more Al are in coordinate 3 (q^3)
 540 than in coordinate 2 (q^2) [104, 105] in these systems, giving them a better stability toward acids

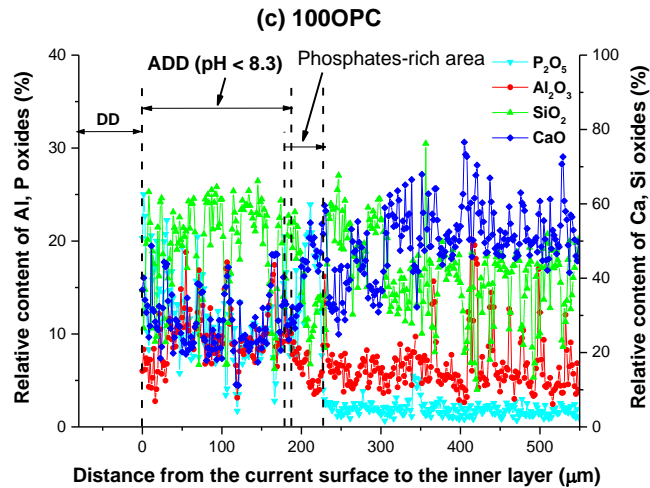
541 compared to Na and Ca [106]. The higher concentrations of Al and Si also confirms an
542 aluminosilicate type gel formed in the degraded area. In contrast, OPC-based pastes had no
543 such sharp increase in the relative concentration of Al and the changes of Ca or Al were
544 relatively stable.



545



546



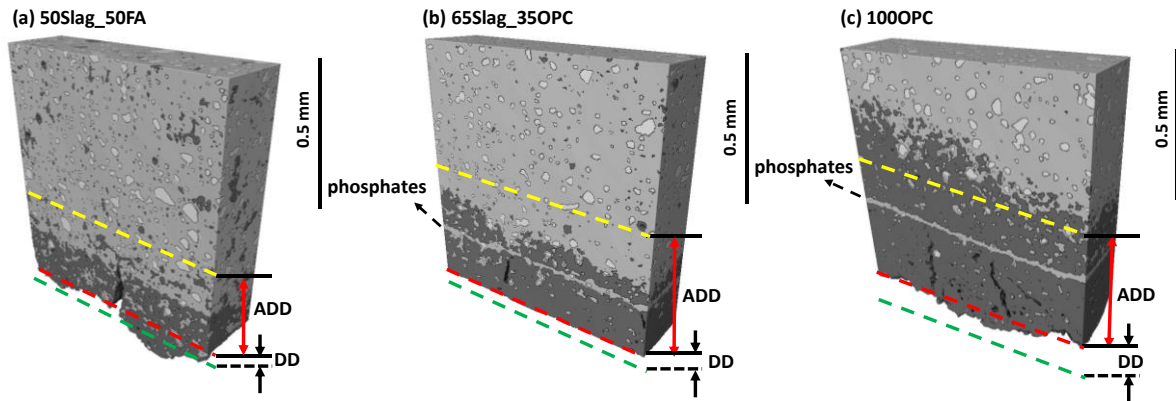
547

548 **Fig. 10.** Chemical analysis of different elements relative content measured by EDS line scan after 14
 549 days of immersion in the phosphoric acid, (a) 50Slag_50FA; (b) 65Slag_35OPC and (c) 100OPC.

550 **Micro-CT analysis**

551 Three dimensional images of the three mixes after 21 days of acid immersion are shown in
 552 Fig. 11 and corresponding ADD and DD values based on Fig. 3 are also provided. Similar to
 553 SEM images, light-grey areas refer to undegraded components with fewer pores and more
 554 unreacted particles (higher density) whereas darker grey areas represent phases containing
 555 more pores and fewer unreacted particles (lower density) meaning they are already partially or
 556 completely degraded. The resolution was 1.78 μm in this study.

557 For 50Slag_50FA and 65Slag_35OPC samples, it is apparent that the binders remain more
 558 or less undegraded (light grey) even when the pH is lower than 8.3 (within the ‘ADD’ area),
 559 which is not the case for 100OPC. Oppositely, the 100 OPC sample displayed some degraded
 560 parts where the pH is still above 8.3 (outside of ‘ADD’ area). This result is in consistent with
 561 the pH stability of different components in the corresponding binders. For 100OPC, the main
 562 components including Ca(OH)₂, ettringite and C-S-H all disappear when pH is lower than 10.5
 563 and thus degraded part is present even when pH is still above 8.3 [26]. In comparison, less
 564 soluble and mechanically sound aluminosilicate gel even after exposure to acids with pH at 3
 565 [27, 107] in 50Slag_50FA and 65Slag_35OPC (also rich in C-(A)-S-H) explains why phases
 566 within ‘ADD’ were still stable. A light grey layer can be observed in the degraded part of the
 567 two OPC-based binders, which is assumed to be different phosphates.



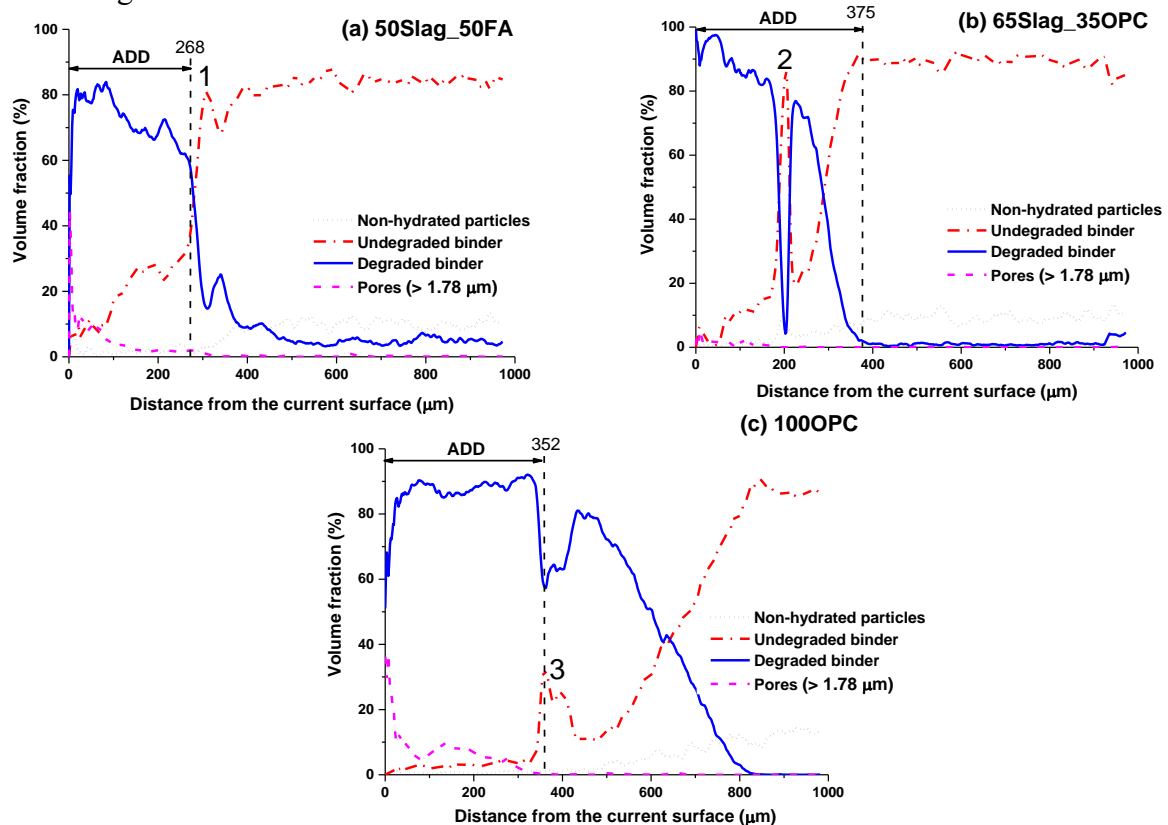
568
569
570
571
572

Fig. 11. 3D micro-CT images of the samples after 21-day exposure towards the phosphoric acid: (a) 50Slag_50FA; (b) 65Slag_35OPC and (c) 100OPC. DD and ADD are also labelled based on the experimental results. Green dashed lines refer to the original surfaces of pastes.

573
574
575
576
577
578
579
580
581

Different volume fractions of the phases in the corresponding mixes based on the 3D images after segmentation and data processing procedure are presented in Fig. 12. The four types of components are determined based on their different relative densities obtained from Fig. 11. ADD values are also included to correlate different components with pH values of pores. The number '1', '2' and '3' indicate the main location of the precipitated phosphates because the undegraded binder experienced an abrupt increase in volume fraction as approaching to the surface which is assumed to be the phosphates with a higher density than the degraded binder. It is also apparent that the undegraded binder maintained a certain volume even within the 'ADD' region.

582
583
584
585
586
587
588
589
590
591



592 **Fig. 12.** Volume fractions of different components in three mixes after 21 days of immersion for (a)
 593 50Slag_50FA, (b) 65Slag_35OPC and (c) 100OPC obtained from the current surface of the sample
 594 derived from micro-CT analysis. The ADD values are obtained from Fig. 3.

595 **3.4. Dissolution rate of powdered samples**

596 The results of Dissolution Rate (DR) and Normalized Dissolution Rate (NDR) are listed in
 597 Table 5. It is found that 100OPC got the largest NDR (0.087 g/m^2) followed by 65Slag_35FA
 598 (0.046 g/m^2) and 50Slag_50FA (0.041 g/m^2). Based on the previous dissolved depth (DD) as
 599 shown in Fig. 3(b), NDR and DD are consistent with each other: compared to the much larger
 600 NDR and DD for 100OPC, the two values for 65Slag_35FA and 50Slag_50FA are close with
 601 each other. The only difference is the immersion condition, one is powdered samples exposed
 602 to nitric acid and another one is cylindrical bulk samples immersed in the phosphoric acid.
 603 Therefore, the consistent results imply that both NDR and DD can be used to reflect the
 604 intrinsic chemical resistance of different binders having no influence of the following two
 605 factors: one is porous media in bulk samples (e.g. tortuosity and connectivity) [108, 109] and
 606 another is precipitations of various salts that may further block the surface or inner pores of
 607 samples, leading to some changes in degradation processes [110]. Similar to DD, the NDR of
 608 different binders reflects the intrinsic stability of various binding gels which is also likely due
 609 to the different Al and Ca contents: a higher aluminum but lower calcium content leads to a
 610 lower NDR.

611 **Table 5**

612 Detailed information on the dissolution rate test (48 hours of immersion for different powder
 613 mixes in the nitric acid solution).

Sample ID	Averaged M_{before} (g)	Averaged M_{after} (g)	S (m^2/g)	DR	NDR (g/m^2)
50Slag_50FA	0.2002	0.0940	13.07	0.53	0.041
65Slag_35FA	0.1998	0.0058	20.90	0.97	0.046
100OPC	0.2000	0.0195	10.39	0.90	0.087

614 Note: M_{before} -the mass of the powdered sample before exposure, M_{after} -the mass of the powdered sample
 615 after exposure, S -BET surface area, DR-Dissolution rate, NDR-Normalized dissolution rate.

617 **4. Conclusions**

618 This study demonstrates the early-stage behaviour of a type of AASF and two types of OPC-
 619 based binders exposed to phosphoric acid ($\text{pH} = 2$) in terms of their degradation kinetics and

620 related microstructural and mineralogical changes. A higher degradation rate was observed in
621 the OPC-based binders, especially the 100OPC specimens. The AASF binder with GGBFS/FA
622 at 1:1 exhibited an ‘induction stage’ within about 7-day degradation depth evolution, which is
623 attributed to its higher neutralisation capacity. Using the leaching data, the calcium content in
624 the binder composition is the most sensitive component of the binder towards acid attack
625 whereas other elements as Al and Si seem relatively stable or negligibly affected. Hence,
626 alternative binders, as here AASF, with a higher content of Al and Si displayed stronger
627 resistance against the phosphoric acid, compared to the 100OPC. The stable highly crosslinking
628 C-(A)-S-H, in the AASF led to the formation of a thicker transition zone which is beneficial
629 for resisting further acid migration and also provides a solid space for the precipitation of
630 different salts such as Brushite. In comparison, 100OPC binder had almost no transition zone
631 and the main components were already partially degraded even when the pH was still higher
632 than 8.3 due to a much higher calcium content introduced by OPC in the binding matrix. The
633 calcium is released at the expense of losing structural integrity, facilitating more ingress of
634 hydronium ions.

635 65Slag_35OPC seemed to present an intermediate behaviour between 50Slag_50FA and
636 100OPC pastes: it had the largest ADD value due to its lowest neutralisation capacity, similar
637 to that of the 100OPC. However, it displayed a transition zone because of a relatively lower Ca
638 content and higher content of Al and Si, leading to a similar DD as that of the 50Slag_50FA
639 binder. Thus, it can be considered as an acceptable alternative to pure OPC binders.

640 Considering the initial highest capillary sorptivity of 50Slag_50FA and highest water
641 absorption as well as VPV of 65Slag_35OPC prior to the acid immersion, it is concluded that
642 the chemistry and structure of the gel formed in each cement has significantly more influence
643 than their microstructural properties in determining the early-stage degradation performance.

644

645 **Acknowledgements**

646 The authors deliver great thanks to Chinese Scholarship Council (CSC), the Geopolymer
647 and Mineral Processing Group laboratory in the University of Melbourne for financial and
648 infrastructure support. This study was also supported by Mrs Laura Jukes who provided great
649 help during the experimental parts. Thank you for the ARC Research Hub for Nanoscience-
650 based Construction Material Manufacturing (IH150100006) for financial support.

651 **References**

- 652 [1] T.A. Aiken, W. Sha, J. Kwasny, M.N. Soutsos, Resistance of geopolymer and Portland cement based
653 systems to silage effluent attack, *Cement and Concrete Research* 92 (2017) 56-65.
- 654 [2] S. Pavía, E. Condren, Study of the durability of OPC versus GGBS concrete on exposure to silage
655 effluent, *Journal of materials in civil engineering* 20(4) (2008) 313-320.
- 656 [3] M.G.D. Gutiérrez-Padilla, A. Bielefeldt, S. Ovtchinnikov, M. Hernandez, J. Silverstein, Biogenic
657 sulfuric acid attack on different types of commercially produced concrete sewer pipes, *Cement and*
658 *Concrete Research* 40(2) (2010) 293-301.
- 659 [4] A. Parande, P. Ramsamy, S. Ethirajan, C. Rao, N. Palanisamy, Deterioration of reinforced concrete
660 in sewer environments, *Proceedings of the Institution of Civil Engineers-Municipal Engineer*, Thomas
661 Telford Ltd, 2006, pp. 11-20.
- 662 [5] L. Zhang, P. De Schryver, B. De Gussemé, W. De Muynck, N. Boon, W. Verstraete, Chemical and
663 biological technologies for hydrogen sulfide emission control in sewer systems: a review, *Water*
664 *research* 42(1-2) (2008) 1-12.
- 665 [6] J. Ren, L. Zhang, R.S. Nicolas, Degradation of Alkali-Activated Slag and Fly Ash Mortars under
666 Different Aggressive Acid Conditions, *Journal of Materials in Civil Engineering* 33(7) (2021).
- 667 [7] K. Scrivener, N. De Belie, Bacteriogenic sulfuric acid attack of cementitious materials in sewage
668 systems, *Performance of cement-based materials in aggressive aqueous environments*, Springer2013,
669 pp. 305-318.
- 670 [8] J. Ren, L. Zhang, R. San Nicolas, Degradation process of alkali-activated slag/fly ash and Portland
671 cement-based pastes exposed to phosphoric acid, *Construction and Building Materials* 232 (2020)
672 117209.
- 673 [9] Y. Xie, X. Lin, T. Ji, Y. Liang, W.J.C. Pan, B. Materials, Comparison of corrosion resistance mechanism
674 between ordinary Portland concrete and alkali-activated concrete subjected to biogenic sulfuric acid
675 attack, 228 (2019) 117071.
- 676 [10] H.B. Chang, Y.C.J.J.o.M.R. Choi, Technology, Accelerated performance evaluation of repair
677 mortars for concrete sewer pipes subjected to sulfuric acid attack, 9(6) (2020) 13635-13645.
- 678 [11] A. Özcan, M.B.I.I.J.o.C.E. Karakoç, The resistance of blast furnace slag-and ferrochrome slag-based
679 geopolymer concrete against acid attack, 17(10) (2019) 1571-1583.
- 680 [12] M. Vafaei, A. Allahverdi, P. Dong, N.J.C. Bassim, B. Materials, Acid attack on geopolymer cement
681 mortar based on waste-glass powder and calcium aluminate cement at mild concentration, 193 (2018)
682 363-372.
- 683 [13] P. Sturm, G. Gluth, C. Jäger, H. Brouwers, H.-C.J.C. Kühne, C. Research, Sulfuric acid resistance of
684 one-part alkali-activated mortars, 109 (2018) 54-63.
- 685 [14] H.A. Khan, A. Castel, M.S. Khan, A.H.J.C. Mahmood, C. research, Durability of calcium aluminate
686 and sulphate resistant Portland cement based mortars in aggressive sewer environment and sulphuric
687 acid, 124 (2019) 105852.
- 688 [15] A. Bertron, J. Duchesne, G. Escadeillas, Degradation of cement pastes by organic acids, *Materials*
689 *and structures* 40(3) (2007) 341-354.
- 690 [16] S. Larreur-Cayol, A. Bertron, G. Escadeillas, Degradation of cement-based materials by various
691 organic acids in agro-industrial waste-waters, *Cement and Concrete Research* 41(8) (2011) 882-892.
- 692 [17] O. Oueslati, J. Duchesne, The effect of SCMs and curing time on resistance of mortars subjected
693 to organic acids, *Cement and Concrete Research* 42(1) (2012) 205-214.
- 694 [18] M. Alexander, C. Fourie, Performance of sewer pipe concrete mixtures with portland and calcium
695 aluminate cements subject to mineral and biogenic acid attack, *Materials and structures* 44(1) (2011)
696 313-330.
- 697 [19] T. Gutberlet, H. Hilbig, R.E. Beddoe, Acid attack on hydrated cement — Effect of mineral acids on
698 the degradation process, *Cement and Concrete Research* 74 (2015) 35-43.
- 699 [20] E. Galanos, K. Gray, A. Biddlestone, K. Thayanithy, The aerobic treatment of silage effluent:
700 effluent characterization and fermentation, *Journal of agricultural engineering research* 62(4) (1995)
701 271-279.

702 [21] M.M. Gebrehanna, R.J. Gordon, A. Madani, A.C. VanderZaag, J.D. Wood, Silage effluent
703 management: A review, *Journal of Environmental Management* 143 (2014) 113-122.

704 [22] J. Ren, S. Guo, J. Su, T. Zhao, J. Chen, S. Zhang, A novel TiO₂/Epoxy resin composited geopolymer
705 with great durability in wetting-drying and phosphoric acid solution, *Journal of Cleaner Production*
706 227 (2019) 849-860.

707 [23] M. Secco, G.I. Lampronti, M.-C. Schlegel, L. Maritan, F. Zorzi, Degradation processes of reinforced
708 concretes by combined sulfate–phosphate attack, *Cement and Concrete Research* 68 (2015) 49-63.

709 [24] J. Ren, L. Zhang, R. San Nicolas, Degradation of alkali-activated slag/fly ash mortars under different
710 aggressive acid conditions, *Journal of materials in civil engineering* (2020).

711 [25] H. Yuan, P. Dangla, P. Chatellier, T. Chaussadent, Degradation modelling of concrete submitted to
712 sulfuric acid attack, *Cement and Concrete Research* 53 (2013) 267-277.

713 [26] R.E. Beddoe, H.W. Dörner, Modelling acid attack on concrete: Part I. The essential mechanisms,
714 *Cement and Concrete Research* 35(12) (2005) 2333-2339.

715 [27] S.A. Bernal, E.D. Rodríguez, R. Mejía de Gutiérrez, J.L. Provis, Performance of alkali-activated slag
716 mortars exposed to acids, *Journal of Sustainable Cement-Based Materials* 1(3) (2012) 138-151.

717 [28] R.R. Lloyd, J.L. Provis, J.S.J. van Deventer, Acid resistance of inorganic polymer binders. 1.
718 Corrosion rate, *Materials and Structures* 45(1) (2012) 1-14.

719 [29] S. Zhang, A. Keulen, K. Arbi, G. Ye, Waste glass as partial mineral precursor in alkali-activated
720 slag/fly ash system, *Cement and Concrete Research* 102 (2017) 29-40.

721 [30] T. Yang, H. Zhu, Z. Zhang, X. Gao, C. Zhang, Q. Wu, Effect of fly ash microsphere on the rheology
722 and microstructure of alkali-activated fly ash/slag pastes, *Cement and Concrete Research* 109 (2018)
723 198-207.

724 [31] X. Gao, Q. Yu, H. Brouwers, Reaction kinetics, gel character and strength of ambient temperature
725 cured alkali activated slag–fly ash blends, *Construction and Building Materials* 80 (2015) 105-115.

726 [32] K. Goretta, N. Chen, F. Gutierrez-Mora, J. Routbort, G. Lukey, J. Van Deventer, Solid-particle
727 erosion of a geopolymer containing fly ash and blast-furnace slag, *Wear* 256(7-8) (2004) 714-719.

728 [33] A. Wardhono, D.W. Law, A. Strano, The strength of alkali-activated slag/fly ash mortar blends at
729 ambient temperature, *Procedia Engineering* 125 (2015) 650-656.

730 [34] A.R. Brough, A. Atkinson, Sodium silicate-based, alkali-activated slag mortars: Part I. Strength,
731 hydration and microstructure, *Cement and Concrete Research* 32(6) (2002) 865-879.

732 [35] T.A. Aiken, J. Kwasny, W. Sha, M.N. Soutsos, Effect of slag content and activator dosage on the
733 resistance of fly ash geopolymer binders to sulfuric acid attack, *Cement and Concrete Research* 111
734 (2018) 23-40.

735 [36] A. Bertron, G. Escadeillas, J. Duchesne, Cement pastes alteration by liquid manure organic acids:
736 chemical and mineralogical characterization, *Cement and Concrete Research* 34(10) (2004) 1823-1835.

737 [37] F. Puertas, S. Martínez-Ramírez, S. Alonso, T. Vazquez, Alkali-activated fly ash/slag cements:
738 strength behaviour and hydration products, *Cement and concrete research* 30(10) (2000) 1625-1632.

739 [38] F. Puertas, A. Fernández-Jiménez, Mineralogical and microstructural characterisation of alkali-
740 activated fly ash/slag pastes, *Cement and Concrete composites* 25(3) (2003) 287-292.

741 [39] I. Ismail, S.A. Bernal, J.L. Provis, R. San Nicolas, S. Hamdan, J.S.J. van Deventer, Modification of
742 phase evolution in alkali-activated blast furnace slag by the incorporation of fly ash, *Cement and*
743 *Concrete Composites* 45 (2014) 125-135.

744 [40] A. Adam, Strength and durability properties of alkali activated slag and fly ash-based geopolymer
745 concrete, School of Civil, Environmental and Chemical Engineering, RMIT University, 2009.

746 [41] N. Lee, H. Lee, Influence of the slag content on the chloride and sulfuric acid resistances of alkali-
747 activated fly ash/slag paste, *Cement and Concrete Composites* 72 (2016) 168-179.

748 [42] W. Zhang, X. Yao, T. Yang, Z. Zhang, The degradation mechanisms of alkali-activated fly ash/slag
749 blend cements exposed to sulphuric acid, *Construction and Building Materials* 186 (2018) 1177-1187.

750 [43] D.M. Roy, W. Jiang, M.R. Silsbee, Chloride diffusion in ordinary, blended, and alkali-activated
751 cement pastes and its relation to other properties, *Cement and Concrete Research* 30(12) (2000) 1879-
752 1884.

753 [44] I. Ismail, S.A. Bernal, J.L. Provis, S. Hamdan, J.S. van Deventer, Drying-induced changes in the
754 structure of alkali-activated pastes, *Journal of Materials Science* 48(9) (2013) 3566-3577.

755 [45] ASTM C642, Standard test method for density, absorption, and voids in hardened concrete, ASTM
756 International, 100 Barr Harbor Drive, PO Box C700, West Conshohocken, PA 19428–2959, United
757 States, 2008.

758 [46] C. ASTM, 1585-04. Standard test method for measurement of rate of absorption of water by
759 hydraulic-cement concretes, ASTM International (2004).

760 [47] A. ASTM, C109/C109M-Standard Test Method for Compressive Strength of Hydraulic Cement
761 Mortars (Using 2-in. or (50-mm) Cube Specimens); 2013. 2, Scope of work shall include but not be
762 limited to the following:-Suspended metal grid for acoustical tile ceiling system (1999).

763 [48] T. Bakharev, Resistance of geopolymer materials to acid attack, *Cement and Concrete Research*
764 35(4) (2005) 658-670.

765 [49] L.T. Angenent, K. Karim, M.H. Al-Dahhan, B.A. Wrenn, R. Domínguez-Espinosa, Production of
766 bioenergy and biochemicals from industrial and agricultural wastewater, *TRENDS in Biotechnology*
767 22(9) (2004) 477-485.

768 [50] S. Wallah, B.V. Rangan, Low-calcium fly ash-based geopolymer concrete: Long-term properties,
769 Curtin University of Technology, 2006.

770 [51] Y. Zuo, M. Nedeljković, G. Ye, Pore solution composition of alkali-activated slag/fly ash pastes,
771 *Cement and Concrete Research* 115 (2019) 230-250.

772 [52] B. Huber, H. Hilbig, M.M. Mago, J.E. Drewes, E. Müller, Comparative analysis of biogenic and
773 chemical sulfuric acid attack on hardened cement paste using laser ablation-ICP-MS, *Cement and*
774 *Concrete Research* 87 (2016) 14-21.

775 [53] C. Magniont, M. Coutand, A. Bertron, X. Cameleyre, C. Lafforgue, S. Beaufort, G. Escadeillas, A
776 new test method to assess the bacterial deterioration of cementitious materials, *Cement and Concrete*
777 *Research* 41(4) (2011) 429-438.

778 [54] A. Bertron, J. Duchesne, G. Escadeillas, Attack of cement pastes exposed to organic acids in
779 manure, *Cement and Concrete Composites* 27(9-10) (2005) 898-909.

780 [55] M. Hossain, M. Karim, M. Hasan, M. Hossain, M.F.M. Zain, Durability of mortar and concrete made
781 up of pozzolans as a partial replacement of cement: A review, *Construction and Building Materials* 116
782 (2016) 128-140.

783 [56] L. Pel, K. Kopinga, E.F. Kaasschieter, Saline absorption in calcium-silicate brick observed by NMR
784 scanning, *Journal of Physics D: Applied Physics* 33(11) (2000) 1380.

785 [57] M. Fournier, M. Odorico, E. Nicoleau, A. Ull, P. Frugier, S. Gin, Reactive Surface of Glass Particles
786 Under Aqueous Corrosion, *Procedia Earth and Planetary Science* 17 (2017) 257-260.

787 [58] S.S. International Organization for Standardization. Technical Committee ISO/TC 24. Particle
788 characterization including sieving, Particle characterization, Determination of the Specific Surface
789 Area of Solids by Gas Adsorption: BET Method, ISO2010.

790 [59] E.C. Arvaniti, M.C. Juenger, S.A. Bernal, J. Duchesne, L. Courard, S. Leroy, J.L. Provis, A. Klemm, N.
791 De Belie, Determination of particle size, surface area, and shape of supplementary cementitious
792 materials by different techniques, *Materials and Structures* 48(11) (2015) 3687-3701.

793 [60] J.L. Bell, P.E. Driemeyer, W.M. Kriven, Formation of ceramics from metakaolin - based
794 geopolymers. Part II: K - based geopolymer, *Journal of the American Ceramic Society* 92(3) (2009)
795 607-615.

796 [61] D.K. Panesar, J. Francis, Influence of limestone and slag on the pore structure of cement paste
797 based on mercury intrusion porosimetry and water vapour sorption measurements, *Construction and*
798 *Building Materials* 52 (2014) 52-58.

799 [62] A. Koenig, A. Herrmann, S. Overmann, F. Dehn, Resistance of alkali-activated binders to organic
800 acid attack: Assessment of evaluation criteria and damage mechanisms, *Construction and Building*
801 *Materials* 151 (2017) 405-413.

802 [63] J.J. Beaudoin, V. Ramachandran, A new perspective on the hydration characteristics of cement
803 phases, *Cement and Concrete research* 22(4) (1992) 689-694.

804 [64] H.M. Jennings, Refinements to colloid model of CSH in cement: CM-II, *Cement and Concrete*
805 *Research* 38(3) (2008) 275-289.

806 [65] A.J. Allen, J.J. Thomas, H.M. Jennings, Composition and density of nanoscale calcium–silicate–
807 hydrate in cement, *Nature materials* 6(4) (2007) 311.

808 [66] C. Varga, M. Alonso, R.M. De Gutierrez, J. Mejía, F. Puertas, Decalcification of alkali-activated slag
809 pastes. Effect of the chemical composition of the slag, *Materials and Structures* 48(3) (2015) 541-555.

810 [67] N. Ukrainczyk, O. Vogt, E.A. Koenders, Reactive transport numerical model for durability of
811 geopolymer materials, *Adv. Chem. Eng. Sci.* 6(04) (2016) 355.

812 [68] P. Rajan, S. Rajendran, J. Sathiyabama, J.L. Christy, J. Jeyasundari, P. Prabhakar, Corrosion
813 inhibitors for concrete corrosion-An Overview, *European Chemical Bulletin* 2(1) (2012) 1-8.

814 [69] R. Vera, M. Villarroel, A. Carvajal, E. Vera, C. Ortiz, Corrosion products of reinforcement in
815 concrete in marine and industrial environments, *Materials Chemistry and Physics* 114(1) (2009) 467-
816 474.

817 [70] M. Kouřil, P. Novák, M. Bojko, Threshold chloride concentration for stainless steels activation in
818 concrete pore solutions, *Cement and Concrete Research* 40(3) (2010) 431-436.

819 [71] P. Feng, C. Miao, J.W. Bullard, A model of phase stability, microstructure and properties during
820 leaching of portland cement binders, *Cement and Concrete Composites* 49 (2014) 9-19.

821 [72] A. Mehta, R. Siddique, Sulfuric acid resistance of fly ash based geopolymer concrete, *Construction*
822 *and Building Materials* 146 (2017) 136-143.

823 [73] S. Thokchom, Fly ash geopolymer pastes in sulphuric acid, *Int. J. Eng. Innovation Res* 3(6) (2014)
824 943-947.

825 [74] O. Oueslati, J. Duchesne, Resistance of blended cement pastes subjected to organic acids:
826 Quantification of anhydrous and hydrated phases, *Cement and Concrete Composites* 45 (2014) 89-
827 101.

828 [75] N.M. Ukrainczyk, M.; Vogt, O.; Koenders, E, Geopolymer, Calcium Aluminate, and Portland
829 Cement-Based Mortars: Comparing Degradation Using Acetic Acid, *materials* 12 (2019) 3115.

830 [76] Li, Zihui, Peethamparan, Sulapha, Leaching resistance of alkali-activated slag and fly ash mortars
831 exposed to organic acid.

832 [77] A. Fernández - Jiménez, F. Puertas, I. Sobrados, J. Sanz, Structure of calcium silicate hydrates
833 formed in alkaline - activated slag: influence of the type of alkaline activator, *Journal of the American*
834 *Ceramic Society* 86(8) (2003) 1389-1394.

835 [78] S.-D. Wang, K.L. Scrivener, Hydration products of alkali activated slag cement, *Cement and*
836 *Concrete Research* 25(3) (1995) 561-571.

837 [79] M.B. Haha, G. Le Saout, F. Winnefeld, B. Lothenbach, Influence of activator type on hydration
838 kinetics, hydrate assemblage and microstructural development of alkali activated blast-furnace slags,
839 *Cement and Concrete Research* 41(3) (2011) 301-310.

840 [80] C.R. Shearer, J.L. Provis, S.A. Bernal, K.E. Kurtis, Alkali-activation potential of biomass-coal co-fired
841 fly ash, *Cement and Concrete Composites* 73 (2016) 62-74.

842 [81] L. Alarcon-Ruiz, G. Platret, E. Massieu, A. Ehlacher, The use of thermal analysis in assessing the
843 effect of temperature on a cement paste, *Cement and Concrete research* 35(3) (2005) 609-613.

844 [82] A. Fernández - Jiménez, A. Palomo, J.Y. Pastor, A. Martin, New cementitious materials based on
845 alkali - activated fly ash: performance at high temperatures, *Journal of the American Ceramic Society*
846 91(10) (2008) 3308-3314.

847 [83] H. El Didamony, H.H. Assal, T.M. El Sökkary, H.A. Abdel Gawwad, Kinetics and physico-chemical
848 properties of alkali activated blast-furnace slag/basalt pastes, *HBRC Journal* 8(3) (2012) 170-176.

849 [84] H.F. Taylor, *Cement chemistry*, Thomas Telford 1997.

850 [85] M.A. Salih, N. Farzadnia, A.A. Abang Ali, R. Demirboga, Development of high strength alkali
851 activated binder using palm oil fuel ash and GGBS at ambient temperature, *Construction and Building*
852 *Materials* 93 (2015) 289-300.

853 [86] M. Thiery, G. Villain, P. Dangla, G. Platret, Investigation of the carbonation front shape on
854 cementitious materials: effects of the chemical kinetics, *Cement and Concrete Research* 37(7) (2007)
855 1047-1058.

856 [87] N.Y. Mostafa, S.A.S. El-Hemaly, E.I. Al-Wakeel, S.A. El-Korashy, P.W. Brown, Characterization and
857 evaluation of the hydraulic activity of water-cooled slag and air-cooled slag, *Cement and Concrete*
858 *Research* 31(6) (2001) 899-904.

859 [88] C. Ruiz-Santaquiteria, J. Skibsted, A. Fernández-Jiménez, A. Palomo, Alkaline solution/binder ratio
860 as a determining factor in the alkaline activation of aluminosilicates, *Cement and Concrete Research*
861 42(9) (2012) 1242-1251.

862 [89] F. Puertas, M. Palacios, A. Gil-Maroto, T. Vázquez, Alkali-aggregate behaviour of alkali-activated
863 slag mortars: Effect of aggregate type, *Cement and Concrete Composites* 31(5) (2009) 277-284.

864 [90] J.A. Gadsden, *Infrared spectra of minerals and related inorganic compounds*, Butterworths 1975.

865 [91] M.B. Haha, B. Lothenbach, G. Le Saout, F. Winnefeld, Influence of slag chemistry on the hydration
866 of alkali-activated blast-furnace slag—Part II: Effect of Al₂O₃, *Cement and Concrete Research* 42(1)
867 (2012) 74-83.

868 [92] M. Ben Haha, G. Le Saout, F. Winnefeld, B. Lothenbach, Influence of activator type on hydration
869 kinetics, hydrate assemblage and microstructural development of alkali activated blast-furnace slags,
870 *Cement and Concrete Research* 41(3) (2011) 301-310.

871 [93] R.L. Frost, S.J. Palmer, Thermal stability of the 'cave' mineral brushite CaHPO₄·2H₂O—Mechanism
872 of formation and decomposition, *Thermochimica acta* 521(1-2) (2011) 14-17.

873 [94] Q. Zhou, F.P. Glasser, Thermal stability and decomposition mechanisms of ettringite at < 120 C,
874 *Cement and Concrete Research* 31(9) (2001) 1333-1339.

875 [95] A. Chaipanich, T. Nochaiya, Thermal analysis and microstructure of Portland cement-fly ash-silica
876 fume pastes, *Journal of Thermal Analysis and Calorimetry* 99(2) (2009) 487-493.

877 [96] A.W. Decho, Overview of biopolymer-induced mineralization: What goes on in biofilms?,
878 *Ecological Engineering* 36(2) (2010) 137-144.

879 [97] B. Lothenbach, G. Le Saout, E. Gallucci, K. Scrivener, Influence of limestone on the hydration of
880 Portland cements, *Cement and Concrete Research* 38(6) (2008) 848-860.

881 [98] M. Zajac, A. Rossberg, G. Le Saout, B. Lothenbach, Influence of limestone and anhydrite on the
882 hydration of Portland cements, *Cement and Concrete Composites* 46 (2014) 99-108.

883 [99] B. Dilnesa, B. Lothenbach, G. Le Saout, G. Renaudin, A. Mesbah, Y. Filinchuk, A. Wichser, E.
884 Wieland, Iron in carbonate containing AFm phases, *Cement and Concrete Research* 41(3) (2011) 311-
885 323.

886 [100] T. Nochaiya, W. Wongkeo, K. Pimraksa, A. Chaipanich, Microstructural, physical, and thermal
887 analyses of Portland cement-fly ash-calcium hydroxide blended pastes, *Journal of thermal analysis*
888 *and calorimetry* 100(1) (2009) 101-108.

889 [101] N. Marjanović, M. Komljenović, Z. Baščarević, V. Nikolić, R. Petrović, Physical-mechanical and
890 microstructural properties of alkali-activated fly ash-blast furnace slag blends, *Ceramics International*
891 41(1, Part B) (2015) 1421-1435.

892 [102] A. Bertron, J. Duchesne, G. Escadeillas, Accelerated tests of hardened cement pastes alteration
893 by organic acids: analysis of the pH effect, *Cement and Concrete Research* 35(1) (2005) 155-166.

894 [103] J. Temuujin, A. Minjigmaa, M. Lee, N. Chen-Tan, A. van Riessen, Characterisation of class F fly
895 ash geopolymer pastes immersed in acid and alkaline solutions, *Cement and Concrete Composites*
896 33(10) (2011) 1086-1091.

897 [104] N. Lee, H. Lee, Reactivity and reaction products of alkali-activated, fly ash/slag paste,
898 *Construction and Building Materials* 81 (2015) 303-312.

899 [105] S.M. Park, J.G. Jang, N. Lee, H.-K. Lee, Physicochemical properties of binder gel in alkali-activated
900 fly ash/slag exposed to high temperatures, *Cement and Concrete Research* 89 (2016) 72-79.

901 [106] S.A. Bernal, J.L. Provis, B. Walkley, R. San Nicolas, J.D. Gehman, D.G. Brice, A.R. Kilcullen, P.
902 Duxson, J.S.J. van Deventer, Gel nanostructure in alkali-activated binders based on slag and fly ash,
903 and effects of accelerated carbonation, *Cement and Concrete Research* 53 (2013) 127-144.

- 904 [107] M. Königsberger, J. Carette, Validated hydration model for slag-blended cement based on
905 calorimetry measurements, *Cement and Concrete Research* 128 (2020) 105950.
- 906 [108] B. Johannesson, Nonlinear transient phenomena in porous media with special regard to concrete
907 and durability, *Advanced Cement Based Materials* 6(3-4) (1997) 71-75.
- 908 [109] J.S. Van Deventer, J.L. Provis, P. Duxson, Technical and commercial progress in the adoption of
909 geopolymer cement, *Minerals Engineering* 29 (2012) 89-104.
- 910 [110] L. De Windt, P. Devillers, Modeling the degradation of Portland cement pastes by biogenic
911 organic acids, *Cement and Concrete Research* 40(8) (2010) 1165-1174.

912

913

914

915